JOURNAL OF GEOPHYSICAL RESEARCH, VOL. 101, NO. D6, PAGES 10,129–10,149, APRIL 30, 1996

Validation of UARS microwave limb sounder 183 GHz H_2O Measurements

W. A. Lahoz,[1,2] M. R. Suttic,[1] L. Froidevaux,[3] R. S. Harwood,[1] C. L. Lau,[4] T. A. Lungu,[3] G. E. Peckham,[4] H. C. Pumphrey,[1] W. G. Read,[3] Z. Shippony,[3] R. A. Suttie,[4] J. W. Waters,[3] G E. Nedoluha,[5] S. J. Oltmans,[6] J. M. Russell III,[7] and W. A. Traub[8]

Abstract. The Upper Atmosphere Research Satellite (UARS) microwave limb sounder (MLS) makes measurements of thermal emission at 183.3 GHz which are used to infer the concentration of water vapor over a pressure range of 46 - 0.2 hPa ($\sim$ 20 to $\sim$ 60 km). We provide a validation of MLS H_2O by analyzing the integrity of the measurements, by providing an error characterization, and by comparison with data from other instruments. It is estimated that version 3 MLS H_2O retrievals are accurate to within 20–25 % in the lower stratosphere and to within 8–13 % in the upper stratosphere and lower mesosphere. The precision of a single profile is estimated to be $\sim$ 0.15 parts per million by volume (ppmv) in the midstratosphere and 0.2 ppmv in the lower and upper stratosphere. In the lower mesosphere the estimate of a single profile precision is 0.25–0.45 ppmv. During polar winter conditions, H_2O retrievals at 46 hPa can have a substantial contribution from climatology. The vertical resolution of MLS H_2O retrievals is $\sim$ 5 km.

1. Introduction

The Upper Atmosphere Research Satellite (UARS) was launched on September 12, 1991 carrying a payload to measure the chemistry, dynamics, and energy balance of the middle atmosphere [*Reber,* 1990]. This paper concerns the data validation of middle atmosphere distributions of H_2O as measured by the microwave limb sounder (MLS) [*Barath et al.,* 1993; *Waters,* 1993].

The MLS instrument is a joint US-UK experiment employing a three-radiometer design, with a 183-GHz radiometer built in the UK that measures H_2O using the emission from the 183.3-GHz H_2O line and O_3 using the emission of the 184.4-GHz O_3 line. For details of the spectroscopy of these two lines, see *Waters* [1976, 1993]. This paper discusses the MLS H_2O measurements and their validation, concentrating on the version 3 MLS data files, the first version to be made publicly available. Companion papers describe the calibration of the MLS instrument [*Jarnot et al.,* this issue], the "forward model" (W. G. Read et al., manuscript in preparation), and validation of MLS ClO [*Waters et al.,* this issue], O_3 [*Froidevaux et al.,* this issue] and temperature and tangent-point pressure [*Fishbein et al.,* this issue]. *Froidevaux et al.* [this issue] give a description of the general algorithms used for retrieving parameters from the calibrated MLS radiances.

In the following sections we provide validation of MLS H_2O data by discussing data processing and the integrity of the radiances used in the retrieval process, by performing an error analysis and by making comparisons between MLS H_2O and other measurements. On the basis of these studies we provide estimates of the accuracy and precision of MLS H_2O data. We also discuss outstanding issues and further work associated with this data set.

[1] Edinburgh University, Edinburgh, Scotland.
[2] CGAM, Reading University, Reading, England.
[3] Jet Propulsion Laboratory, Pasadena, California.
[4] Heriot-Watt University, Edinburgh, Scotland.
[5] Naval Research Laboratory, Washington, D.C.
[6] NOAA Climate Monitoring and Diagnostic Laboratory, Boulder, Colorado.
[7] NASA Langley Research Center, Hampton, Virgina.
[8] Harvard-Smithsonian Centre for Astrophysics, Cambridge, Massachusetts.

Paper number 95JD01703.
0148-0227/96/95JD-01703$05.00

2. MLS version 3 Data Processing

The output of the 183-GHz radiometer is down-converted through an intermediate frequency (IF) stage into a 15-channel, 500-MHz-wide filter-bank, centred on the 183.3-GHz line. The measured radiances include the contributions of a primary sideband and an image sideband [*Jarnot et al.,* this issue]. From the intensity and spectral characteristics of this emission and its variation as the MLS field of view (FOV) is scanned vertically across the atmospheric limb, profiles of H_2O are inferred. The width of the MLS FOV half-power points is 3.7 km in the vertical and 7.2 km in the horizontal.

The horizontal resolution along the line of sight (perpendicular to the UARS velocity vector) is $\sim$ 400 km, set by the physics of radiative transfer.

The measurement latitudinal coverage is from 34° on one side of the equator to 80° on the other. UARS yaws around at $\sim$ 36-day intervals (a "UARS month"), when MLS high-latitude coverage switches from one hemisphere to the other. Within each UARS month the UARS orbit precesses slowly with respect to local solar time, so that the measurements sweep through all local solar times during a UARS month, coming $\sim$ 20 min earlier each day at a fixed latitude.

The UARS project has defined four levels of data (level 0 $\rightarrow$ level 3) which represent the data flow from raw telemetry data, level 0, to fields of geophysical parameters on standard grids, levels 3AT, 3AL, and 3B. UARS level 1 data consist of calibrated radiances for each channel, their measurement precisions, and related instrument data. The MLS radiance values are expressed as brightness temperatures in units of degrees Kelvin and have a random uncertainty associated with them. UARS level 2 data consist of geophysical parameters, and numerous diagnostics. The UARS level 2 data are on a grid chosen by each instrument team. MLS level 2 data consist of vertical profiles (the vertical coordinate being $-\log_{10}(p)$, p being pressure in hPa) of geophysical parameters which have a spatial and temporal location associated with them. The retrieval algorithm used to derive level 2 data is based on a combination of a priori and measurement information [*Rodgers,* 1976; *Froidevaux et al.,* this issue] and makes use of the forward model, developed by W. G. Read et al. (manuscript in preparation), to calculate the influence functions (also known as weighting functions). It is clear that the integrity of the level 2 and level 3 data is very dependent on the integrity of the level 1 radiances and considerable effort has been expended in assessing the robustness of these radiances [*Jarnot et al.,* this issue]. More details will be provided in section 3 below.

UARS level 3AT data are geophysical parameters gridded each 65.536-s time interval onto pressure surfaces p_n, where $p_n = 1000 \times 10^{-n/6}$ hPa (n = 0, ..., 42) (which would correspond to a constant height spacing of 2.7 km in an isothermal atmosphere with a constant pressure scale-height of 7 km). Each day contains 1318 or 1319 profiles. The MLS level 3AT retrieved water vapor volume mixing ratio profile is represented as a piecewise-linear function with breakpoints at alternate, even-numbered, UARS pressure surfaces, e.g., at 10, 4.6, 2.2, and 1 hPa. (The MLS level 2 retrieved profiles are similarly represented.) The water vapor mixing ratios on the even-numbered surfaces are the retrieved breakpoint values, while those on the odd-numbered surfaces, e.g., 6.8, 3.2, and 1.5 hPa, are averages of the mixing ratios on adjacent even-numbered surfaces. This means that the vertical resolution of level 3AT H_2O profiles imposed by this representation corresponds to a height resolution of $\sim$ 5.4 km. level 3AL data are like 3AT data except gridded every 4° in latitude and temporal information is lost. There are generally only about 2/3 the number of level 3AT profiles in a level 3AL file, namely, close to 840 profiles. The level 3B data comprise globally mapped representations of 3AL data.

Retrievals of MLS data are constrained with a priori information, with the result that where there is poor information content in the MLS measurements, the retrieved values and their associated uncertainties relax to the a priori values. Consequently, it is important for the retrieval algorithm to have reasonable a priori inputs (values and error information) so that they do not overconstrain or underconstrain the solution.

In the case of MLS the a priori inputs are based on a month-dependent climatology developed by the UARS science team [*Barnett and Corney,* 1989]. The UARS H_2O climatology [*Remsberg et al.,* 1990] consists mainly of monthly zonal means from the limb infrared monitor of the stratosphere (LIMS) [*Russell et al.,* 1984] for 7 months (November to May), 100 to 1.5 hPa and 56°S to 84°N. From 1.5 to 0.5 hPa, radiance-averaged profiles from LIMS data are used. Besides the LIMS data, ground-based microwave data [e.g. *Bevilacqua et al.,* 1985, 1987; *Tsou et al.,* 1988] are used in the mesosphere for pressures of 0.5 to 0.01 hPa. The H_2O UARS climatology was extended to the whole of the year by assuming hemispheric symmetry in the seasons. Extensions where UARS climatology is unavailable make use of default values which were constructed from the Caltech/JPL photochemical model for a midlatitude equinox day. A diagonal a priori error covariance matrix is used. In the stratosphere the assumed a priori uncertainty is set to 2 parts per million by volume (ppmv). By comparison, the standard deviation about the zonal mean of typical LIMS H_2O profiles for May and October tends to be less than 1 ppmv throughout most of the stratosphere [*Remsberg et al.,* 1990]. This strongly suggests that an *a priori* error of 2 ppmv for MLS H_2O retrievals in the stratosphere is large and is unlikely to overconstrain the solution to the input climatology. Tests with significantly larger a priori errors gave results which were negligibly different from the standard retrievals within the useful vertical range of the data.

The uncertainty, σ, associated with each retrieved H_2O profile is computed by the retrieval algorithm and is stored along with the retrieved value in the level 2 and level 3 files as a quality indicator. This uncertainty, which includes contributions from random noise and from certain systematic errors, is obtained by propagating the precisions of the radiance measurements (a level 1 product), the estimates of uncertainties in the constrained parameters and the estimates of inaccuracies in the forward model through the retrieval software. A more detailed discussion of the errors associated with version 3 MLS H_2O retrievals is presented in sections 3 and 4.

At the conclusion of the retrieval the ratio of the estimated uncertainty to its a priori counterpart is formed. This ratio is sometimes termed the "error ratio." When this ratio exceeds 0.5 (that is, the retrieved mixing ratio has a contribution from the climatology which exceeds 25%), the quality is set negative to flag the dependence

of the retrieval on the climatology. Typically, for every profile, this tends to occur at or above the 0.046-hPa retrieval level and below 46 hPa. However, at high latitudes in winter, the ratio can exceed 0.5 at 46 hPa and at 22 hPa (see section 6).

An important feature of the UARS MLS experiment is that it measures O_3 at two different frequencies (184.4 and 206.1 GHz) using two different radiometers (183 and 205 GHz). In regions of the atmosphere where both measurements are sensitive to changes in constituent amount, the availability of two independent O_3 measurements means that intra-MLS comparisons can be carried out and, for example, the consistency of the calibration of the 183 and 205 GHz radiometers can be checked. The version 3 algorithms contain an adjustment to the pointing angle of the 183 GHz radiometer field of view (FOV), based on a comparison between the two ozone retrievals and in-flight calibration involving scans across the disk of the moon [*Froidevaux et al.*, this issue]. This has had an impact on the MLS H_2O distribution, namely, a reduction of $\sim 5\,\%$ in retrieved stratospheric values by comparison with version 2 retrievals.

The MLS radiances can contain an offset, or baseline, which is caused by a variety of effects such as insufficiently accurate modeling of the sidelobes of the antenna FOV. It does not depend on frequency but can change from one tangent height to the next. The baseline is handled by retrieving it along with the water vapor. The a priori value of the baseline is taken to be the retrieved value for the tangent height above the one being retrieved. The a priori uncertainty for the baseline is 3 K. Above 40 km, where there should be little or no signal in the wing channels, the baseline can be retrieved very accurately. It usually has a value of about 2 K at 80 km dropping to 1.5 K at 40 km. In the lower stratosphere, it becomes difficult to distinguish between baseline effects and radiation which is due to water vapor. The retrieved baseline often increases sharply to between 4 K and 8 K in this region. This may be a source of systematic error in the water vapor retrieval in the lower stratosphere and is a subject of current investigation.

The version 3 retrieval algorithm assumes linearity. Accordingly, it is less accurate in regions where the atmosphere is optically thick and the radiative transfer equations are correspondingly nonlinear. The 183.3-GHz H_2O emission line measured by MLS is relatively strong and, consequently, tends to have high opacities throughout the stratosphere: the line center becomes optically thick for levels in and below the upper stratosphere; the wings of this line become optically thick for levels in and below the lower stratosphere. Furthermore, no tropospheric retrievals of H_2O are possible with the 183-GHz radiometer due to limited bandwidth. To prevent the retrieval algorithm from operating in regimes that are non-linear, an 'opacity criterion' [*Froidevaux et al.*, this issue] has been devised to discard measurement information when the estimated optical depth exceeds a value of 1.0.

Investigations on the data quality of version 3 MLS H_2O provide strong evidence that retrievals at the 46-hPa level at high latitudes in winter can have a substantial contribution from the a priori input. Detailed studies indicate that this is due to a combination of the atmosphere being optically thick and the very low temperatures prevailing in these regions (especially in winter), which results in estimated opacities for these cases exceeding the 'opacity criterion' and a consequent loss of information content. In these circumstances, most of the information is contributed from fields of view with tangent pressures less than 46 hPa.

3. Signals and Closure

In this section we discuss the integrity of the radiances measured by band 5 of the MLS 183-GHz radiometer. We present a test of consistency and investigate the extent of closure of these radiances. We also discuss closure issues for the retrieved H_2O mixing ratios by means of simulated retrievals.

3.1. Radiances

An important aspect of validating the MLS H_2O retrievals is the examination of the radiances measured by the instrument. Figure 1 shows calculated limb emission in the spectral region 182–187 GHz which includes both spectral sidebands of band 5 and band 6 (MLS band 6 radiances are used for retrieving O_3 [see *Froidevaux et al.*, this issue]. The position of the local oscillator (LO) at 184.78 GHz is indicated in the plot. Spectra are shown for tangent pressures in both the upper and the lower stratosphere. Spectral lines of all molecules which are thought to be important are included in the calculation employing spectral data from the JPL catalog [*Pickett et al.*, 1992]. The primary (signal) sideband is dominated by the 183.3-GHz H_2O line, whereas the image sideband contains no strong lines, giving a 'clean' measurement of 183 GHz H_2O limb emission. There are 15 spectral channels spanning the 510-MHz bandwidth of band 5. For each channel the sideband ratio, describing the relative response of the primary and image sidebands, has been measured. Details of the bandwidth and frequencies of the channels, of the vertical scan patterns and of the procedures for converting the level 0 data to calibrated radiances and error estimates (level 1 data) are given by *Jarnot et al.* [this issue]. On October 17, 1991, the vertical resolution of the scan pattern was increased in the lower stratosphere to improve measurements in this region.

Typical examples of measured radiances in band 5 are shown in Figures 2 and 3. Vertical profiles of the radiances in channels 1 to 8 are plotted in Figure 2. Channel 8 measures the limb emission at the line center and saturates in the primary sideband at tangent heights of ~ 50 km. Between ~ 50 km and ~ 20 km, where the primary sideband of channel 8 is saturated and there is no significant signal in the image sideband, variations in that radiance reflect variations in the temperature of the atmosphere. For channel 1, on the wing

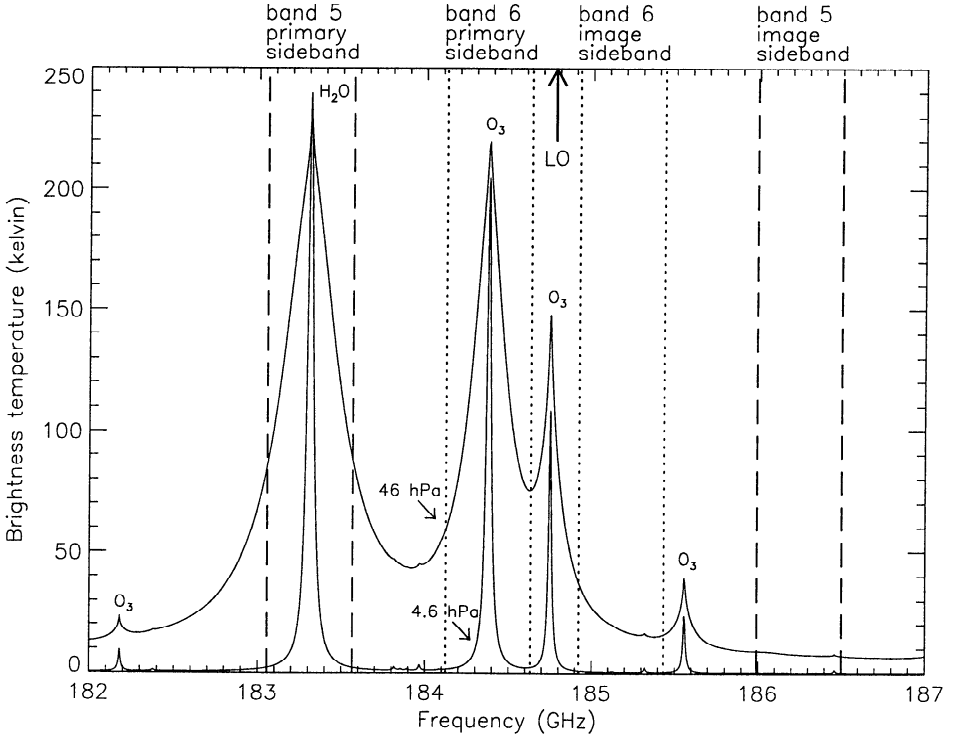

Figure 1. Calculated limb emission in the spectral region 182–187 GHz which includes both spectral sidebands of microwave limb sounder (MLS) band 5 (vertical dashed lines) and band 6 (vertical dotted lines). The position of the 183-GHz radiometer local oscillator (LO) at 184.78 GHz is indicated. Spectra for tangent pressures of 46 and 4.6 hPa are plotted.

of the 183.3-GHz line, the signal in the primary sideband is not significant until the FOV is scanned down to tangent heights of $\sim$ 30 km. The signal in the image sideband begins to make a significant contribution in all channels at $\sim$ 20 km. The three panels in Figure 3 display typical measured spectra in the mesosphere, upper stratosphere, and lower stratosphere. The width of each channel is depicted by a horizontal bar and the 1σ measurement uncertainty is represented by a vertical bar. The effect of pressure broadening is clearly seen as the tangent pressure increases.

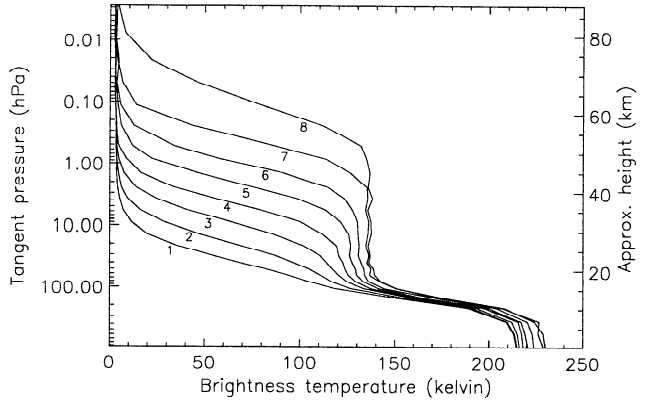

Figure 2. MLS band 5 (183 GHz H_2O) limb radiance profiles for channels 1–8 for a tropical profile (4.25°N, 334.99°E) on January 10, 1992.

3.2. Internal Consistency

In an isothermal atmosphere, when a spectral channel is saturated, the radiance in that channel should represent the blackbody emission for the temperature of the atmosphere and is insensitive to the amount of atmospheric constituent. One test of consistency of the measured radiances is to compare them with the retrieved temperatures for a profile which is nearly isothermal. Figure 4 shows the radiances for such a profile, with the temperature also plotted and scaled by the sideband ratio. The radiances behave qualitatively as expected; all channels appear to saturate within 10 K of a brightness temperature of approximately 125 K. The center channels saturate at a slightly higher temperature because the profile is not quite isothermal; the temperature increases slightly with height. The saturation is less clear in the wing channels because the image sideband starts to receive radiation at tangent heights where the principal sideband is not saturated.

It is clear, however, that the measured radiances tend to saturate at a brightness temperature between 5 and 10 K higher than the temperature profile would lead one to expect. Approximately 1 K of this discrepancy is due to a systematic bias in the MLS temperature retrieval (see *Fishbein et al.*, this issue); another 2 K is the baseline. The rest is possibly due to inexact knowledge of the sideband ratios. The effect this would have on the version 3 retrieval is small, because radiances close to saturation are not used, while those far from saturation

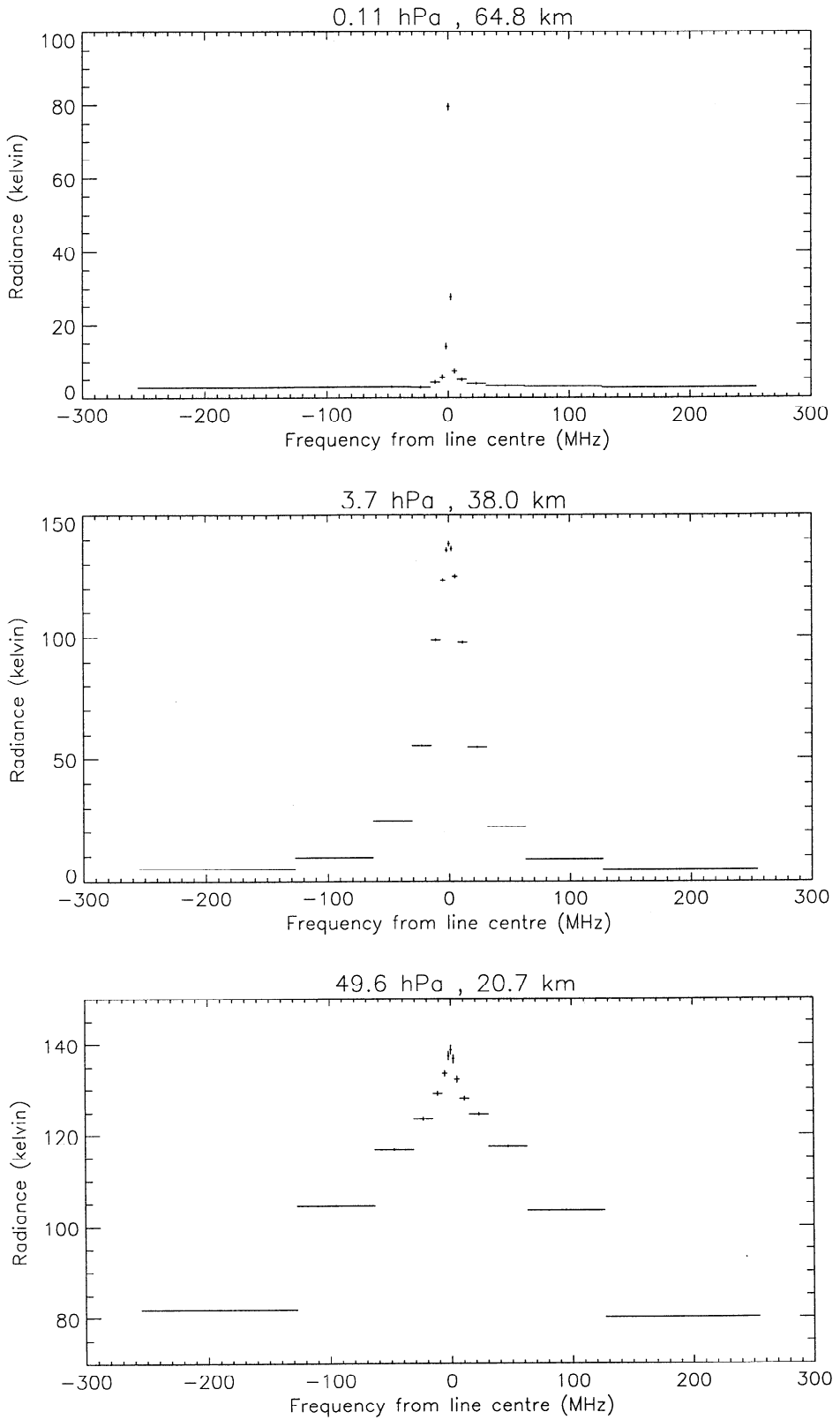

Figure 3. MLS band 5 (183 GHz H_2O) radiance spectra for a tropical profile (4.25°N, 334.99°E) on January 10, 1992 at three tangent pressures: (top) 0.11 hPa, (middle) 3.7 hPa, and (bottom) 50 hPa.

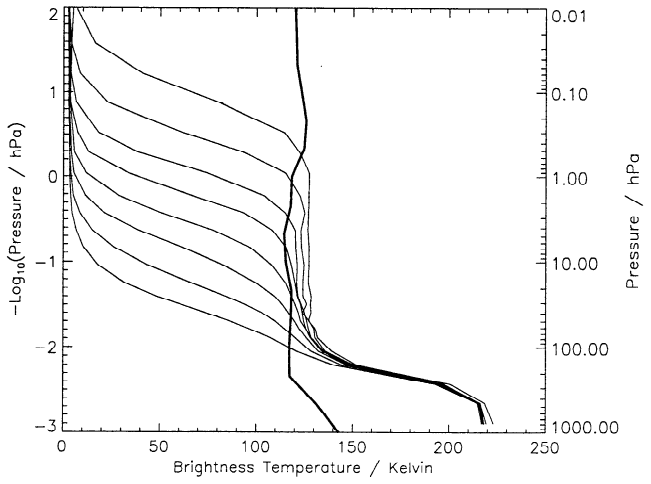

Figure 4. Radiances from channels 1 to 8 for a MLS scan at latitude 56.05°N, longitude 255.13°E on January 10, 1992. Also shown, by the thick curve, is the MLS temperature profile, scaled by the 0.58 sideband ratio. Note that the baseline is about 2 K; the radiances tend to this value as height increases.

are not too sensitive to sideband ratio. However, it is necessary that we resolve this discrepancy before a full nonlinear retrieval can be carried out.

3.3. Closure in Radiances

Another test of a retrieval scheme is the extent to which radiances calculated from the retrieved product agree with the measured radiances within the expected noise. Discrepancies larger than instrument noise indicate a lack of adequate fit to the measured radiances and indicate some type of systematic error. The source of this error could either be in the retrieved product or in the forward model which calculated the radiances. We define the radiance residual as the measured radiance minus the calculated radiance, and the nature of the variation of these residuals with respect to height, spectral channel, and location is discussed.

The plots in Figure 5 show typical variations of radiance residual with height, for each of the 15 channels of band 5, for an equatorial location on January 10, 1992. The horizontal bars represent the 1σ measurement noise. The plots in Figure 5 relate to a single profile, but they are representative of the generally observed variation of radiance residual with height. Figures 6 and 7 show plots of average residuals within latitude bands 10°N–10°S and 60°N–80°N, respectively, for January 10, 1992. Each of these figures displays the variation of the average residuals within eight selected pressure bins ranging from 100 to 0.01 hPa. Vertical bars represent the standard error on the mean measured radiance for a particular channel within a particular pressure range and latitude band. In general, this quantity is small and due to the vertical scale of the plots in Figures 6 and 7 these vertical bars are visible in the pressure range 0.032–0.01 hPa only. The number of limb views which were included in each of the calculations of the average residual ranges from around 200 for the pressure range 0.032–0.01 hPa to about 800 for the pressure range 100–31.6 hPa. Within the two latitude bands mentioned above, similar variations of average residual with spectral channel are found, except for channels 7 and 8 in the mesosphere.

The main features of the residuals in Figures 5–7 are as follows: A large negative residual of ~ -15 K (10–15%) appears in all channels at around 15 km (see Figure 5). At this level in the atmosphere the version 3 MLS H_2O retrievals provide essentially no measurement information and a priori abundances are climatological. If the a priori H_2O amount is an overestimate of the truth at around 15 km, then the recalculated radiances will be greater than the measured radiance which would result in a negative residual. This occurs below the lower limit of the useful vertical range for MLS version 3 H_2O retrievals (see section 4).

Referring to Figures 6 and 7, certain systematic patterns are evident in the spectral signature of the residuals. In the lower stratosphere there appears to be an asymmetry in the residuals for the wing channels. In the pressure range 31.6–10 hPa, channels 13, 14, and 15 exhibit negative residuals, whereas the residuals in channels 1, 2 and 3 are positive. Channels 4–11 have positive residuals of between 2 and 4 K (1–4%) in the latitude bin 10°N–10°S and smaller positive residuals of 1–2 K ($\sim$ 1%) in the latitude bin 60°N–80°N. These residual patterns may be the result of a combination of errors in parameters such as the antenna transmission or the relative response of the primary and image sidebands. In the upper stratosphere and lower mesosphere (panels for pressure ranges 10–3.16 hPa, 3.16–1 hPa, and 1–0.32 hPa) there appears to be an oscillatory behavior of the residuals across the band. This signal may be related to errors in the assumed line shape and is under investigation. In the pressure range 0.32–0.1 hPa the residual pattern differs between the latitude bins 10°N–10°S and 60°N–80°N. For this pressure range, channel 9 exhibits a large positive residual in both latitude bins; however, channels 7 and 8 switch from having positive residuals in the range 10°N–10°S to having negative residuals in the 60°N–80°N range. Residuals for ascending and descending parts of orbits were looked at separately to check whether this effect was due to a Doppler shift caused by winds which are not modeled. However, there was no significant difference in the patterns of residuals between ascending and descending sides of the orbits.

In the above we have described the main systematic features which occur in the radiance residuals for MLS version 3 H_2O retrievals. The possible sources of these features, including errors in antenna transmission, assumed line shape, sideband ratios, and the alignment of the field of view are being investigated.

One can define diagnostics of goodness of fit by using the chi-square (χ^2) concepts from statistical analysis [e.g. *Bevington,* 1969]. We have calculated values of

$$\chi^2_{ma} = \frac{1}{N} \sum \frac{(y_i - y_i^c)^2}{\epsilon_i^2} \qquad (1)$$

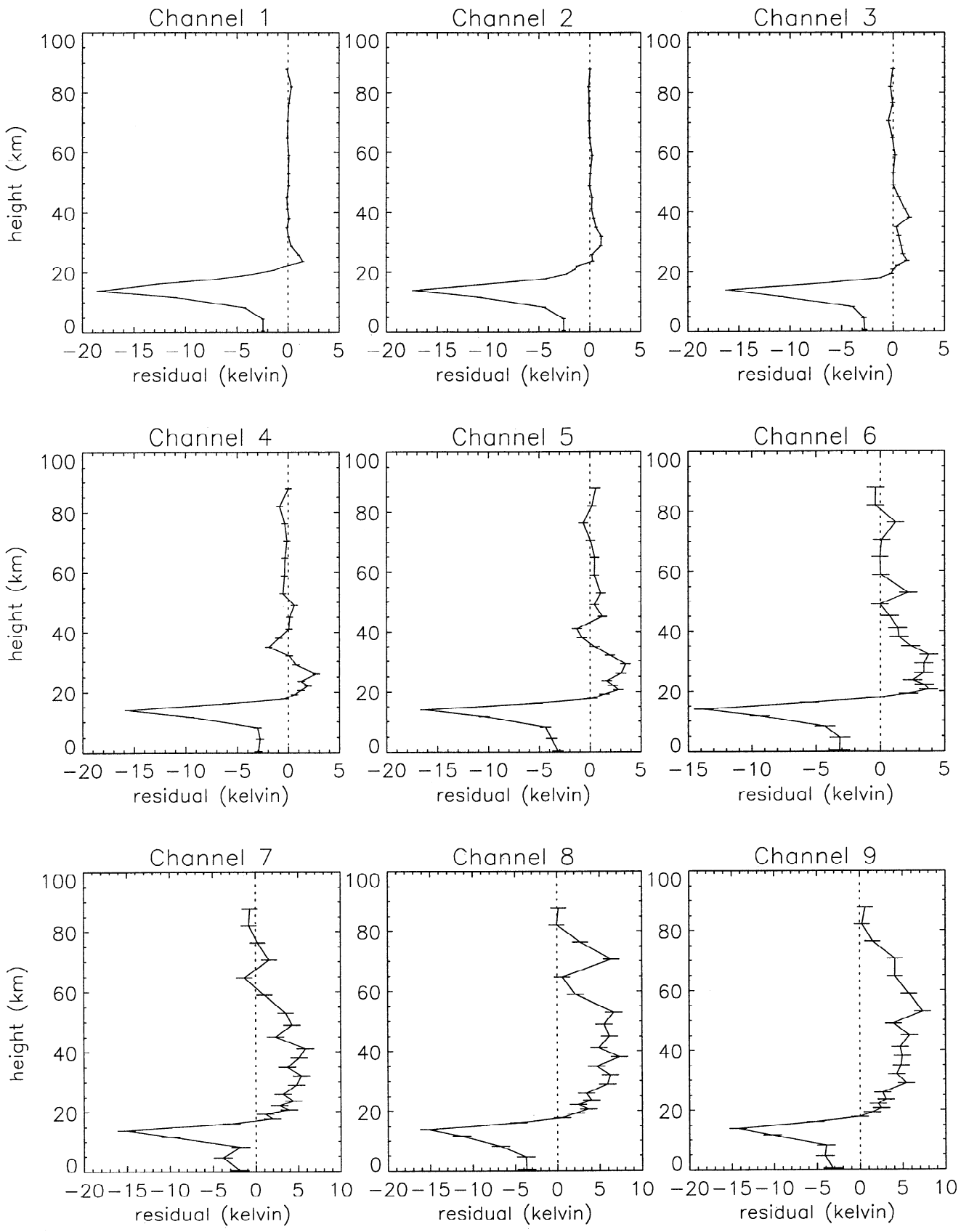

Figure 5. MLS band 5 radiance residual profiles for channels 1–15 for January 10, 1992, at (4.25°N, 334.99°E). The horizontal bars represent the 1σ measurement noise.

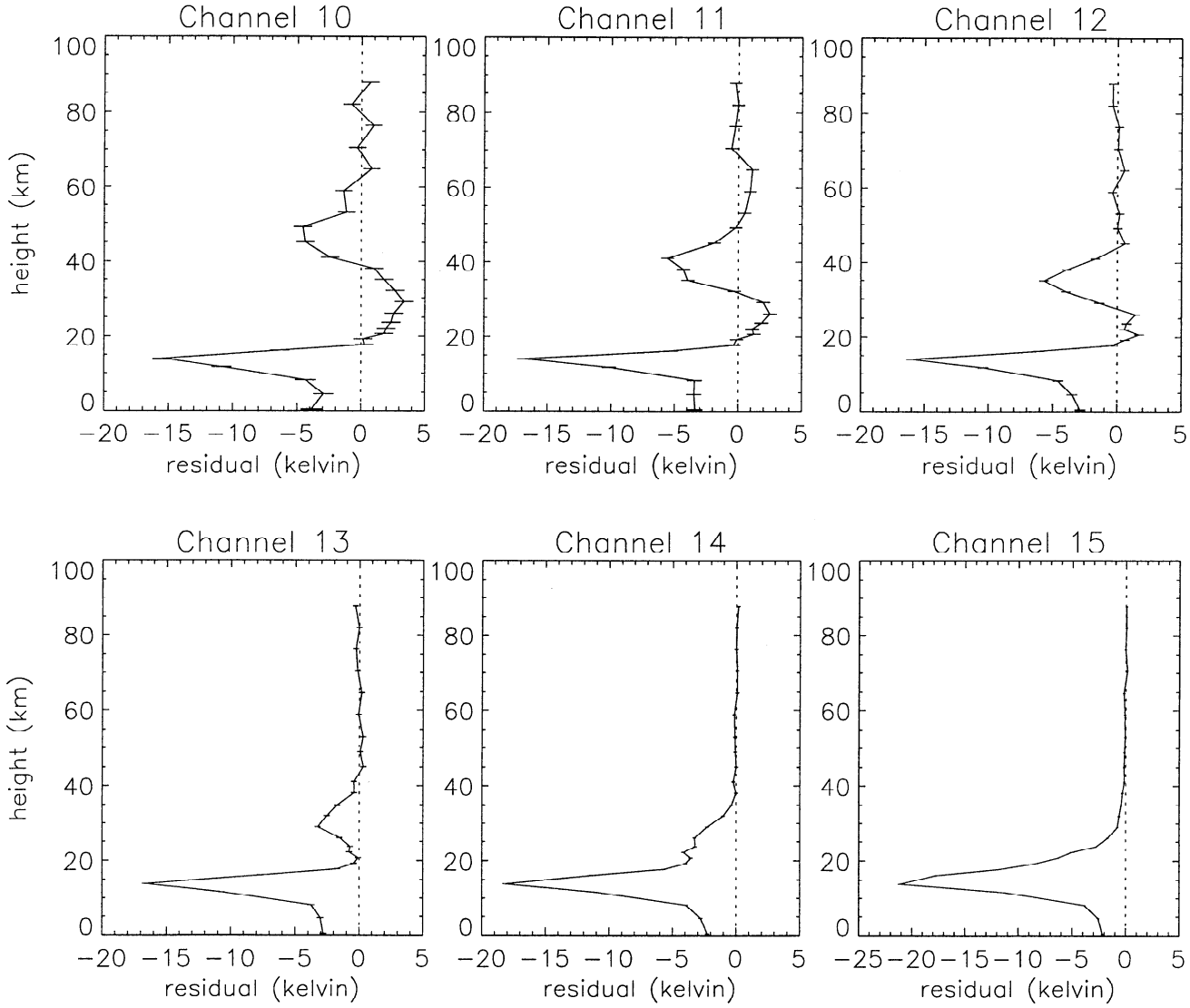

Figure 5. (continued)

for each major frame (one full limb scan). The variables y_i, y_i^c, and ϵ_i refer to measured radiance, calculated radiance (from linear model used in the retrievals), and random (rms) radiance uncertainty, respectively. N is given by the number of degrees of freedom, namely, the total number of observations (radiances) minus the number of parameters being retrieved. The above diagnostic is referred to as a reduced chi-square; in the algorithms used to produce version 3 data files, index i runs over all radiances from the top of the atmosphere to 46-hPa tangent pressure, to avoid too much emphasis on the less well characterized regions in the lowermost stratosphere. A value of χ^2_{ma} above about 2, given the number of degrees of freedom available for each MLS major frame, indicates a significant lack of fit to the radiances within the measurement noise.

Plate 1 shows daily zonal averages of χ^2_{ma} as a function of latitude, over the lifetime of the 183-GHz radiometer. The gaps in June and July 1992 occur when the 183-GHz radiometer was switched off in connection with a problem with the UARS solar array drive. The χ^2_{ma} values range from 12 to 40, indicating that the version 3 data are not limited by measurement noise. This lack of fit to the radiances arises due to a combination of uncertainties in the calibration of the instrument, uncertainties in forward model parameters, and the use of a linear retrieval method and is implied by the radiance residuals discussed above. However, the variation of χ^2_{ma} with time and latitude provides some useful information to the data user. During October 1991 the χ^2_{ma} values are lower than average. This is due to the initial scan sequence containing fewer limb views in the lower stratosphere than the normal scan sequence; the radiance fit is expected to be poorer in the lower stratosphere. The MLS scan sequence used for the remainder of the 183-GHz measurements commenced on October 17, 1991. During August and September 1992 at latitudes poleward of 70°S the χ^2_{ma} values are higher than average, indicating a poorer fit. This is during the southern hemisphere winter and is related to known problems with the MLS version 3 H_2O retrieval at high latitudes in winter (see section 6). From October 1992

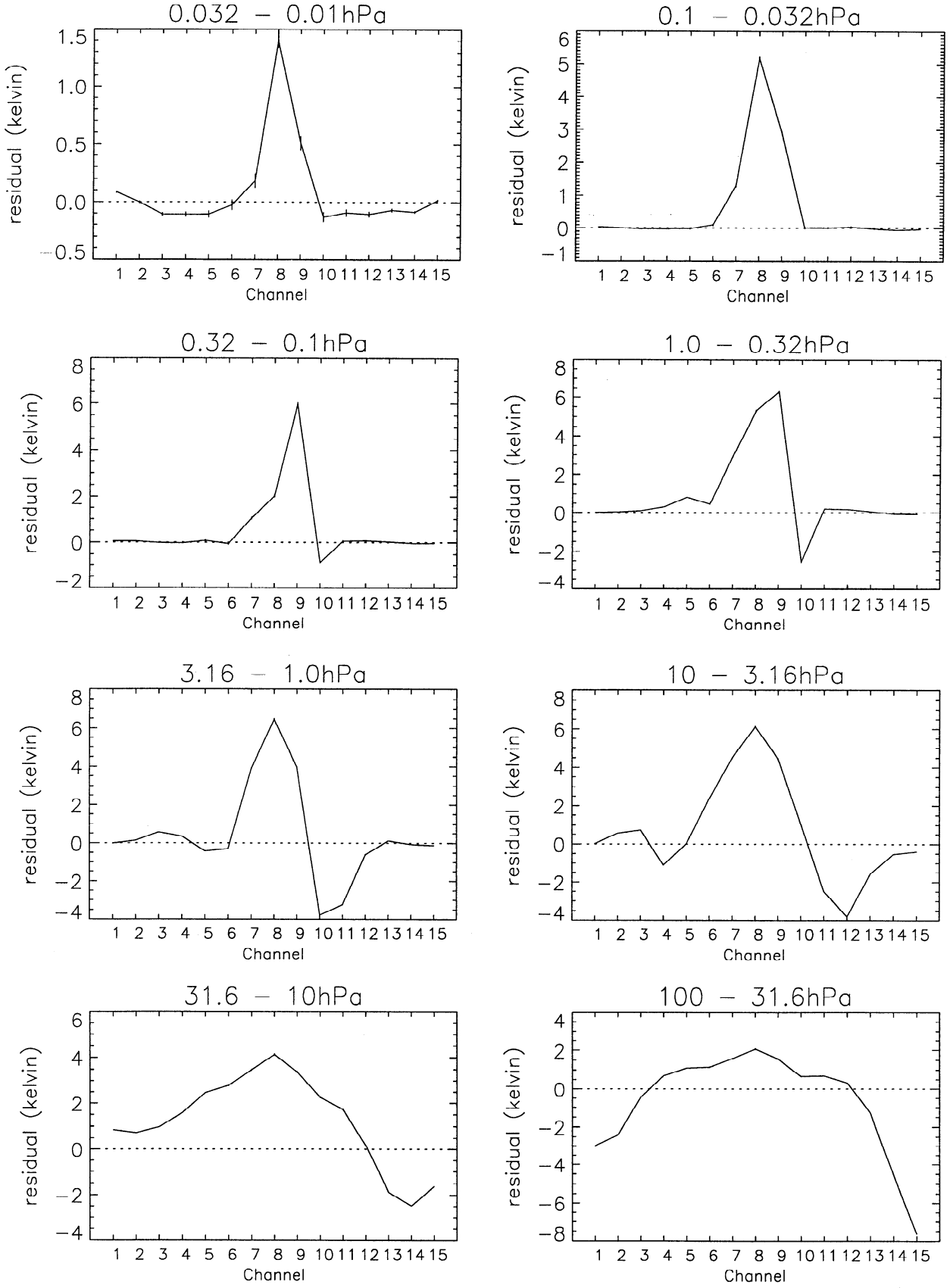

Figure 6. MLS band 5 average radiance residual spectra for January 10, 1992 within latitude band 10°N–10°S. The pressure range is displayed above each panel. Vertical bars represent the standard error on the mean measured radiance. The number of limb views included in the calculation of the average radiance residual ranges from around 200 in the pressure range 0.032–0.01hPa to around 800 in the pressure range 100–31.6hPa.

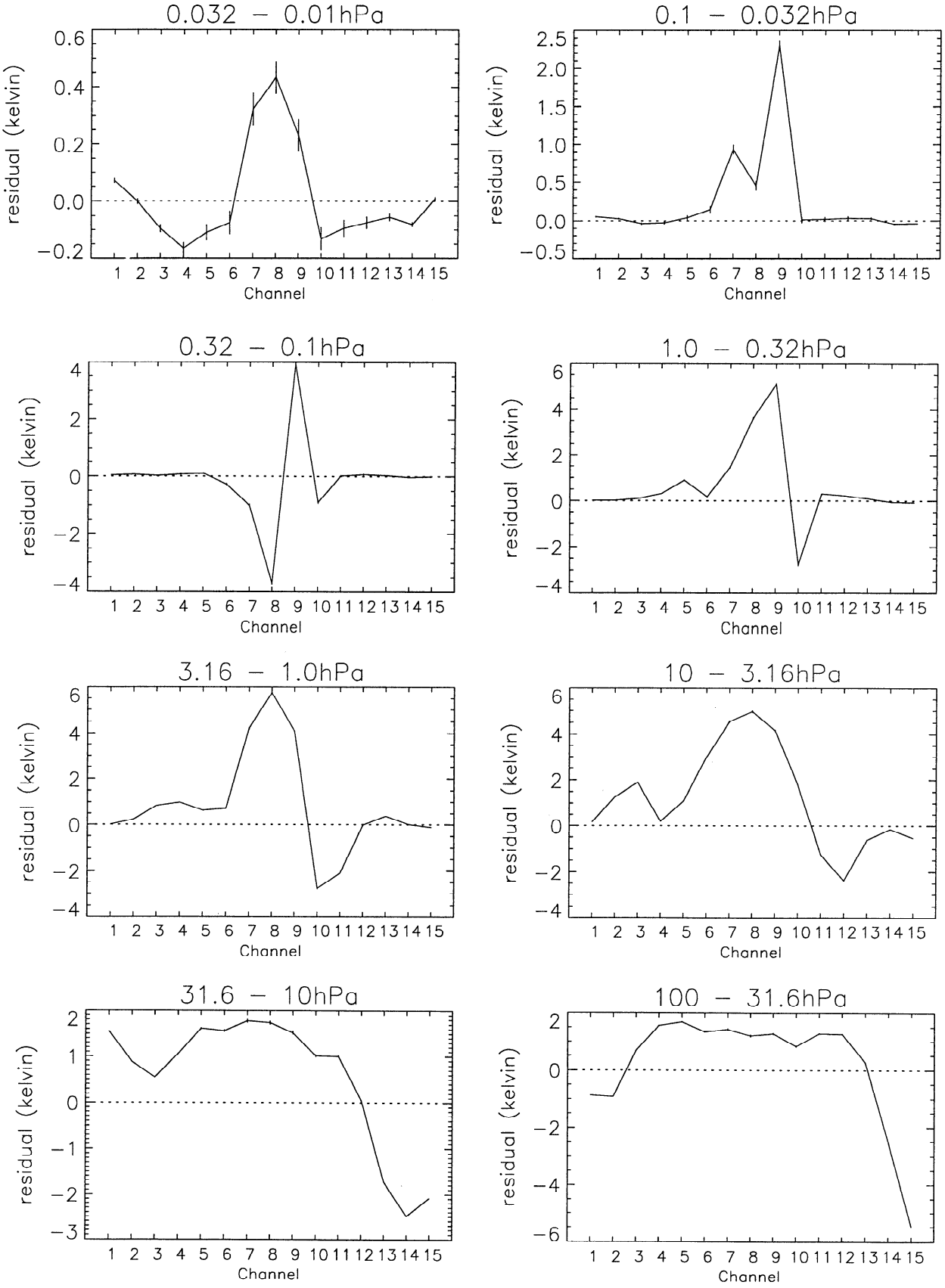

Figure 7. MLS band 5 average radiance residual spectra for January 10, 1992, within latitude band 60°N–80°N. The pressure range is displayed above each panel. Vertical bars represent the standard error on the mean measured radiance. The number of limb views included in the calculation of the average radiance residual ranges from around 200 in the pressure range 0.032–0.01hPa to around 800 in the pressure range 100–31.6hPa.

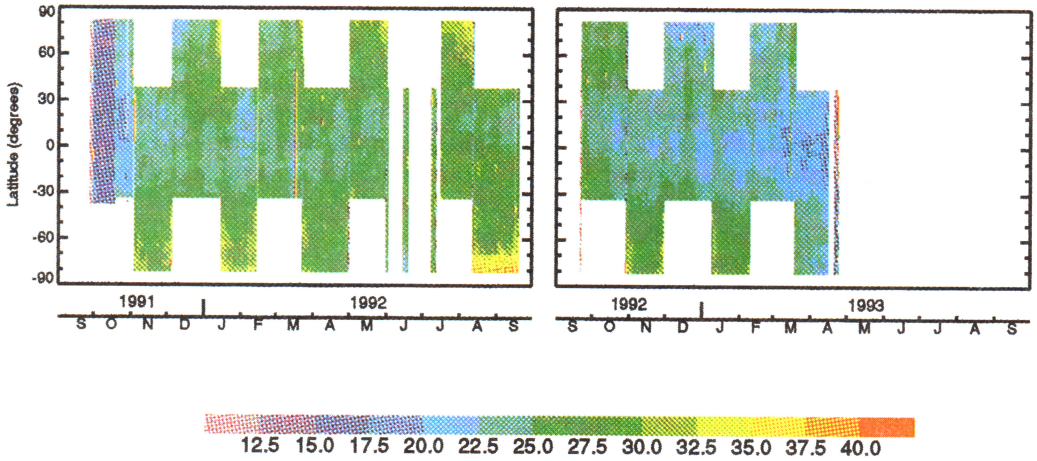

Plate 1. Zonally averaged diagnostic (χ^2_{ma}), as a function of latitude and time, for radiances in the H_2O band (band 5) of the 183 GHz radiometer. (Left) First year of UARS MLS data, (right) second year (no data beyond mid-April from the 183-GHz radiometer). The color bar at the bottom gives the scale for the χ^2_{ma} values.

to April 24, 1993, when the 183-GHz radiometer was turned off, χ^2_{ma} tends to decrease in value. The decreasing χ^2_{ma} values during the latter period of operation are due to the increasing noise on the radiances.

3.4. Closure of retrievals

We now investigate the extent of closure of the MLS version 3 H_2O retrievals in order to estimate the magnitude of "numerical errors" arising from the software used to create the version 3 data files. This involves performing a retrieval using simulated radiances which are calculated from an assumed H_2O distribution. The retrieved H_2O field is then compared with the original (true) field. In this work we have employed a smoothed version of the H_2O distribution as retrieved by MLS for September 17, 1992, as the true distribution. Simulated

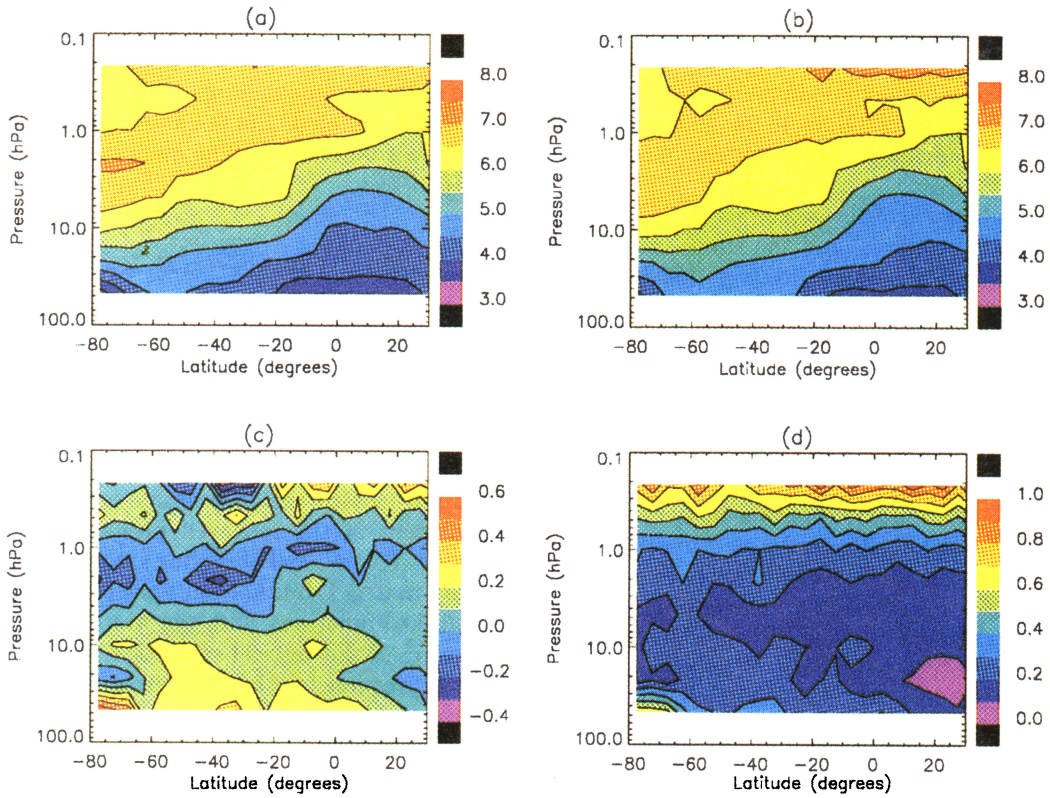

Plate 2. (a) Zonal mean of smoothed H_2O field used to represent the true distribution in tests of retrieval closure, units are parts per million by volume (ppmv) (field taken from MLS version 3 H_2O retrieval for September 17, 1992). (b) Zonal mean of retrieved H_2O using simulated radiances based on the true distribution; units are ppmv. (c) Zonal mean difference (retrieval – truth) H_2O; units are ppmv. (d) The rms difference between retrieval and truth, units are ppmv.

radiances were produced based on this field and these radiances, with simulated noise added, were then used as input to the retrieval. We do not expect perfect closure because the retrieval is based on assumptions of linearity and does not fully utilize the set of radiance measurements when the atmosphere is deemed to be optically thick. This is particularly important for limb views with tangent heights in the lower stratosphere.

The zonal mean of the smoothed H_2O field employed as the true distribution and the zonal mean of the retrieved H_2O field are displayed in Plates 2a and 2b, respectively. The zonal mean difference between these two fields is plotted in Plate 2c, and the root-mean-square (rms) difference is shown in Plate 2d. The vertical range of the plots has been limited from 46 hPa to 0.2 hPa. Below 46 hPa the retrieved values are climatological and above 0.2 hPa there exist known problems with the retrieval (see section 6).

The rms difference between the true and the retrieved H_2O distributions is approximately 0.2 ppmv (2–5 %) throughout the stratosphere with the retrieval having the tendency to overestimate the true distribution in the lower stratosphere. At latitudes greater than 60° (in either hemisphere), on the 46-hPa retrieval surface, the rms difference can be larger than 0.6 ppmv (~ 15 %). This is caused by a loss of measurement information due to estimates of large optical thickness in these regions, and this results in the retrieved values having a substantial contribution from the a priori. Above 1 hPa the zonal mean difference remains at ~ 0.2 ppmv (~ 4 %), but the rms difference increases from ~ 0.3 ppmv (~ 5 %) at 1 hPa to nearly 1 ppmv (~ 12 %) at 0.2 hPa. This is due mainly to an increase in random errors, such as radiance noise and uncertainty in the retrieved temperature, and to an increase in the step size of the FOV scan.

In general, the closure of the retrievals is satisfactory throughout the stratosphere, and the above mentioned features are subjects of current investigation (see section 6). The error analysis presented in section 4 takes account of numerical errors produced by the retrieval process.

4. Estimated Uncertainties

In this section we present the estimated uncertainties for the version 3 MLS H_2O retrievals from band 5 of the 183-GHz radiometer. The estimated uncertainties are based on everything known apart from comparisons with other data sets (see section 5). We also include information on the averaging kernels (defined below) and vertical resolution of the retrievals. Firstly, a brief review of the method of error characterization is given. This is followed by a discussion of the averaging kernels and vertical resolution, and then estimates of the random uncertainties (precision) and systematic uncertainties are presented.

4.1. Characterization method

A general method for estimating the different contributions to the total uncertainty in retrieving an atmospheric constituent profile by any inversion technique is given by *Rodgers* [1990] [see also *Marks and Rodgers,* 1993]. A brief outline of the method is presented below.

If the vector $\mathbf{x}$ represents the true state of the atmosphere and the vector $\hat{\mathbf{x}}$ is the retrieved state, then the total error in a retrieval is given, to first order in small quantities, by

$$\hat{\mathbf{x}}-\mathbf{x} = [T(\bar{\mathbf{x}}, \hat{\mathbf{b}}, \hat{\mathbf{c}})-\bar{\mathbf{x}}]+\mathbf{D}_y\mathbf{K}_b\epsilon_b+\mathbf{D}_y\epsilon_y+(\mathbf{A}-\mathbf{I})(\mathbf{x}-\bar{\mathbf{x}}), \quad (2)$$

where

- $\bar{\mathbf{x}}$ reference state of the atmosphere (for MLS $\bar{\mathbf{x}} = \mathbf{x}_a$, the a priori state);
- $\hat{\mathbf{b}}$ estimate of non-retrieved forward model parameters $\mathbf{b}$;
- $\hat{\mathbf{c}}$ estimate of the inverse model parameters $\mathbf{c}$, e.g. a priori data;
- $\mathbf{K}_b$ known as the model parameter influence function matrix, is the sensitivity of the model radiances to the forward model parameter vector $\mathbf{b}$;
- ϵ_b vector of uncertainties in $\mathbf{b}$;
- ϵ_y measured radiance error vector.

The transfer function T relates the retrieved state $\hat{\mathbf{x}}$ to the unknown true state $\mathbf{x}$ by $\hat{\mathbf{x}} = T(\mathbf{x}, \mathbf{b}, \mathbf{c})$. The contribution function $\mathbf{D}_y$ is the sensitivity of the retrieval to the measurements $\mathbf{y}$. The averaging kernel matrix $\mathbf{A}$ is defined by

$$\mathbf{A} = \frac{\partial \hat{\mathbf{x}}}{\partial \mathbf{x}} = \mathbf{D}_y\mathbf{K}_x,$$

where $\mathbf{K}_x$ is the influence function (also known as the weighting function) matrix of the atmospheric state, i.e., the sensitivity of the model radiances to a change in the state of the atmosphere.

Each row of the matrix $\mathbf{A}$ represents the vector of weights by which the true profile is multiplied to give the element of the retrieved profile corresponding to that row. For an ideal observing system, $\mathbf{A}$ would be the identity matrix $\mathbf{I}$, but normally the rows of $\mathbf{A}$ will represent peaked functions, with the width of the peak being a measure of the vertical resolution of the retrieval.

An expression for the total error covariance $\mathbf{S}_T$ of a retrieval is given, from equation (2), as

$$\mathbf{S}_T = \mathbf{S}_P + \mathbf{S}_M + \mathbf{S}_S,$$

where

$$\begin{aligned} \mathbf{S}_P &= \mathbf{D}_y\mathbf{K}_b\mathbf{S}_b\mathbf{K}_b^T\mathbf{D}_y^T, \\ \mathbf{S}_M &= \mathbf{D}_y\mathbf{S}_\epsilon\mathbf{D}_y^T, \\ \mathbf{S}_S &= (\mathbf{A}-\mathbf{I})\mathbf{S}_a(\mathbf{A}-\mathbf{I})^T. \end{aligned}$$

The matrix $\mathbf{S}_P$ is the contribution to the retrieval error covariance of uncertainties in the model parameters; $\mathbf{S}_b$ is the error covariance matrix for the forward model parameters. The matrix $\mathbf{S}_M$ is the contribution of measurement noise to the retrieval error covariance; $\mathbf{S}_\epsilon$ is the measurement error covariance. The matrix $\mathbf{S}_S$ is known as the "smoothing" error. This can be regarded as the error that comes from the a priori error. The matrix $\mathbf{S}_a$ represents the expected covariance of the departures of the true atmosphere from the a priori profile.

The method outlined in the above paragraphs has been applied to the version 3 H_2O retrieval from band 5 of MLS for a typical midlatitude case. Some important features of the calculations are mentioned and then a discussion of the results of this formal error characterization is given.

The influence functions ($\mathbf{K}$ matrices) were calculated for a typical midlatitude atmosphere using the formulation of W. G. Read et al. (manuscript in preparation), and were evaluated at 43 tangent pressures between $z = -3$ and $z = +4$ inclusively, with a separation in z of 1/6, where z is $-\log_{10}(p)$, p being pressure in hPa. These influence functions were then linearly interpolated onto a typical MLS scan pattern before the error calculations were performed. The retrieval levels chosen for H_2O were the same as those employed by the MLS version 3 retrieval, i.e., 20 levels between $z = -3$ and +3.33 inclusively, with a separation of 1/3.

Typical a priori profile uncertainties used by the MLS retrieval were used to construct a purely diagonal covariance matrix $\mathbf{S}_a$, which therefore assumes that no interlevel correlations are present. The measurement error covariance matrix $\mathbf{S}_\epsilon$ was constructed from typical MLS band 5 radiance errors under the assumption that no interchannel correlations are present. The use of an opacity criterion (see section 2) has also been built into the calculations. When estimating the extent of systematic errors in H_2O mixing ratio, for some systematic effects an equivalent error in radiance was estimated and a corresponding radiance error covariance matrix was constructed, i.e., essentially providing an estimate of $\mathbf{K}_b\mathbf{S}_b\mathbf{K}_b^T$. This error in radiance was then translated into an uncertainty in retrieved H_2O mixing ratio. For other systematic effects an estimate of the root-mean-square (rms) uncertainty in H_2O mixing ratio was given directly from sensitivity studies.

4.2. Averaging Kernels and Vertical Resolution

We now discuss the MLS H_2O averaging kernels. Figure 8 shows the resulting rows of the averaging kernel matrix for the H_2O retrieval at levels $z = -2$ to +3.33. The number printed at the peak of the functions represents the retrieval level, in $\log_{10}(p)$ (pressure in hPa), associated with each averaging kernel.

In general, between $z = -1.67$ and +2 (46–0.01 hPa), the averaging kernels are well-peaked functions with the peak coinciding with the level of the retrieval. In this region, most of the information in the H_2O retrieval comes from the measurements and not from the a priori information. Below $z = -1.67$ (46 hPa), the averaging kernels are not so well peaked because there is little information in the measurements due to the band 5 channels becoming optically thick in this region. Above $z = +2$ (0.01 hPa), the averaging kernels become wider and have smaller peaks due to the decreasing signal-to-noise ratio with altitude and the coarser steps of the FOV scan in this region.

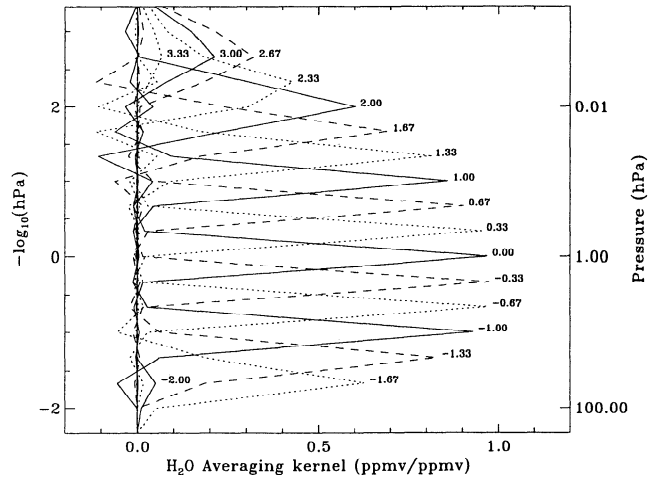

Figure 8. Averaging kernels for MLS version 3 H_2O retrievals.

We note that the averaging kernels shown here were calculated using a representation of the true atmospheric profiles identical to the relatively coarse MLS retrieval grid. However, the true profile is actually continuous, and so any estimate of the amount of smoothing (see Section 4.4) that results from both the measurement technique and the retrieval process may be an underestimate. Work is under way to employ a representation of higher resolution for the true profile when evaluating the averaging kernels.

As an estimate of the vertical resolution of the MLS version 3 H_2O retrievals, the "width" of each averaging kernel has been calculated using the Backus-Gilbert definition of spread [*Backus and Gilbert,* 1970] and is plotted in Figure 9. This gives the vertical resolution between $z = -1.33$ and +0.67 (21.5–0.2 hPa) as $\sim$ 5 km and from $z = +1$ to +2.67 (0.1–0.002 hPa) as $\sim$ 6–10 km. The vertical resolution at $z = -1.67$ (46 hPa) is $\sim$ 6 km.

From the information given by the averaging kernels alone, the useful vertical range for version 3 H_2O retrievals would be 46–0.01 hPa. However, other evidence, namely, frequently occurring high values at $\sim$ 0.1 hPa which seem unrealistic, leads us to believe that the current useful vertical range is 46–0.2 hPa for version 3 data.

4.3. Estimated Precision

We present three methods used to estimate the precision of the H_2O retrievals.

Method 1. This estimate of the precision is based on the formal analysis discussed above. The precision

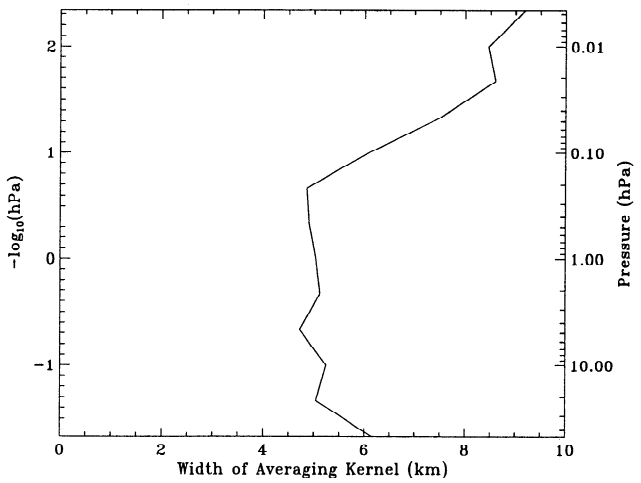

Figure 9. Vertical resolution of MLS version 3 H_2O retrievals.

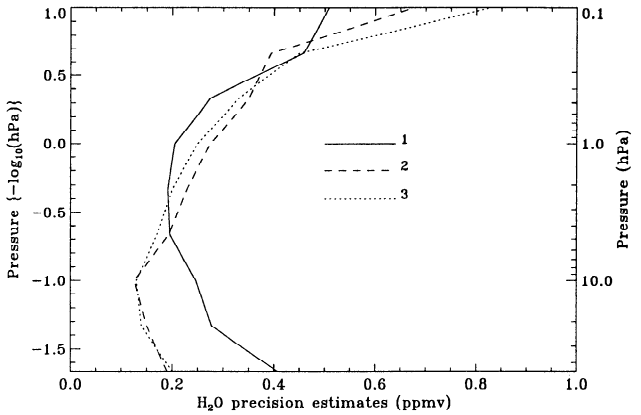

Figure 11. Precision estimates for MLS version 3 H_2O. Method 1: from formal error analysis; method 2, variability of retrieved profiles near to the orbit turning points in the summer hemisphere, method 3, variability of retrieved profiles in the tropics; units are parts per million by volume.

estimate is given by the root-sum-square of the random contributions to the retrieved H_2O uncertainty which includes the measurement noise, the random errors in retrieved temperature and tangent pressure, and uncertainties in other state vector parameters which affect the H_2O retrieval. Figure 10 shows a plot of the dominant random errors together with the root-sum-square (rss) of the random errors. In the lower stratosphere the random error is dominated by the uncertainty in the retrieved tangent pressure. However, the uncertainties in retrieved tangent pressure that are incorporated into the formal error analysis include some systematic effects [*Fishbein et al.*, this issue]. Therefore this method may lead to an overly pessimistic estimate of precision, especially in the lower stratosphere. A comparison of this precision estimate with the precision estimates provided by methods 2 and 3 below is shown in Figure 11.

Method 2. This method involves calculating the variability of retrieved profiles near the orbit turning points (near 80°N or 80°S) in the summer hemisphere. It is at these latitudes that the densest sampling occurs and the summer hemisphere is chosen to minimize any effects from atmospheric variability. Line 2 in Figure 11 shows the rms difference between pairs of profiles near the turning points. These profile pairs are less than 2 hours apart in time and are separated by less than 150 km. The time period used was July 19, 1992 to August 8, 1992 which gave 241 pairs of profiles near to 80°N.

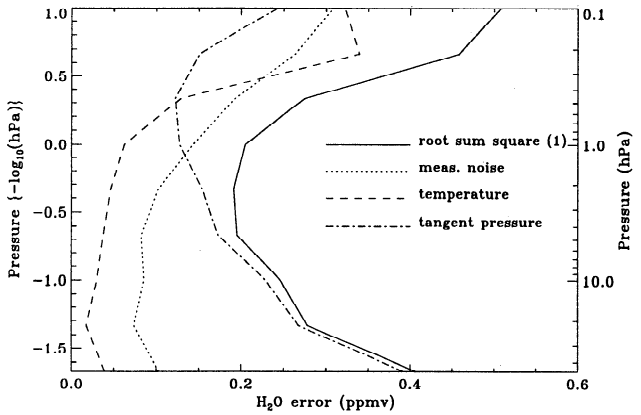

Figure 10. Estimated random errors associated with the retrieval of MLS H_2O; units are ppmv. Line 1 is an estimate of precision given by method 1 of section 4.

Method 3. This method involves calculating the variability of retrieved profiles in the tropics where the atmospheric variability is usually small. Line 3 in Figure 13 shows this estimate of precision. It is a result of calculating the standard deviation of retrieved profiles in the latitude range 5°N–5°S for each one of 442 days and averaging the standard deviations over these days.

Comparing the precision estimates shown in Figure 11 arising from the three methods described above, we can see that methods 2 and 3 give very similar results. Method 1 gives a poorer estimated precision in the lower stratosphere and this may be related to the presence of systematic components in the retrieved tangent pressure uncertainty as mentioned above. An estimate of the precision for the useful vertical range of the H_2O retrievals is given in section 7. Note that the H_2O uncertainties given in the MLS version 3 data files are somewhat greater than the estimates produced by the above methods. This is mainly because the MLS version 3 uncertainties contain a contribution from the a priori error. This effect is strongest in the lower stratosphere. The MLS version 3 errors also contain a systematic component which accounts for known differences between linear and nonlinear retrievals.

4.4. Estimated systematic uncertainties

In addition to random uncertainties, it is necessary to consider systematic uncertainties. Figure 12 shows the dominant systematic uncertainties along with the root-sum-square of all the systematic uncertainties considered. Below, we briefly discuss the various error sources which were considered in this analysis. First, we will

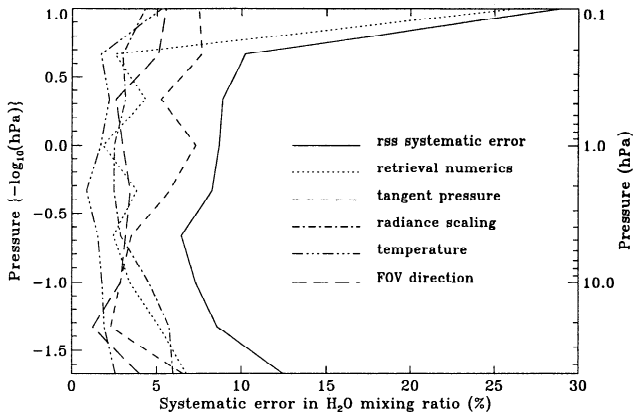

Figure 12. Estimated systematic uncertainties associated with the retrieval of MLS H_2O.

discuss the sources of the dominant systematic uncertainties (see Figure 12).

Tangent pressure. Since the retrieved mixing ratios are based on radiances at the retrieved tangent pressure then errors in tangent pressure can produce errors in mixing ratio. Sensitivity tests were performed assuming a systematic error in tangent pressure of about 6 % [see *Fishbein et al.*, this issue]. The main source of this systematic error is from possible errors in the O_2 spectroscopic database. We can see from Figure 12 that these errors tend to dominate the systematic error between 2 hPa and 0.2 hPa.

Temperature. Errors in temperature can lead to errors in mixing ratio. Sensitivity tests were performed taking biases in temperature to be 2 K for latitudes equatorward of 60° and 5 K for latitudes poleward of 60°. These biases are consistent with observed average differences between MLS and National Meteorological Center (NMC) temperatures [see *Fishbein et al.*, this issue]. Tangent pressure was retrieved while the temperature biases were imposed. The resulting changes in H_2O mixing ratio were then analyzed. At midlatitudes the systematic uncertainty in mixing ratio is generally about 1–2 % for a 2 K systematic error in temperature.

Retrieval numerics. This refers to the differences between the mixing ratio profiles used to create simulated noise-free radiances and the subsequent retrieved profiles based on these radiances using the inversion algorithm. At 0.1 hPa (outside the useful vertical range) this uncertainty is $\sim$ 27 % which may account for the unrealistically high mixing ratios which can sometimes occur at this pressure level.

Radiance scaling. three sources of scaling errors in calibrated radiances are radiometric calibration, sideband ratio errors and spectroscopic errors in linestrength. The first two error sources are discussed by *Jarnot et al.* [this issue]. Based on this reference, we use a systematic uncertainty of 0.6 % for the radiometric calibration of the 183-GHz radiometer which corresponds to about one third of the worst case error expected. This uncertainty is due mainly to uncertainties in the pre-launch characterization of losses through the MLS antenna and switching mirror. A covariance matrix of radiance errors from this source was constructed which assumes the errors are fully correlated across the band and with height. Errors in the sideband ratios can lead to possible errors in single sideband radiance of $\sim$ 2% for the 183-GHz H_2O band [see *Jarnot et al.*, this issue]. These errors should be correlated in some way across the band but because of lack of knowledge of such correlations a covariance matrix of radiance errors was constructed which assumes no correlation is present. This gives a conservative estimate of the resulting uncertainty. For a systematic error in line strength we have assumed a value of 1 % based on *Pickett et al.* [1992] which is probably a conservative estimate of the line strength error. Again, a covariance matrix of radiance errors due to this source was constructed which assumes that the errors are fully correlated across the band and with height. The resulting uncertainties in H_2O due to these three sources were combined by taking the root-sum-square uncertainty.

Field of view (FOV) direction. errors in the FOV direction are related to possible errors in misalignment of the 183-GHz radiometer FOV with respect to the 63-GHz FOV. Postlaunch calibration data from scans of the moon indicate a need for an alignment adjustment of the 183-GHz radiometer FOV from the prelaunch data [see *Jarnot et al.*, this issue]. The MLS version 3 data used a misalignment value of 0.006° which is somewhat less than the result of the studies based on moon-views of 0.011°. We have assumed an uncertainty of 0.007° in FOV direction (this is the uncertainty assumed in the MLS version 3 data) and mapped this uncertainty into H_2O mixing ratio.

The following sources of systematic error were also considered but the resulting uncertainties in mixing ratio are generally not so significant as those which arise from the above-mentioned sources. The uncertainties in mixing ratio from the sources below are not plotted but have been included in the estimate of the root-sum-square systematic uncertainty shown in Figure 14.

Spectroscopy. Errors in spectroscopic parameters can give rise to errors in retrieved mixing ratio. Line positions are known extremely accurately at microwave wavelengths and therefore do not represent a significant error source. Uncertainties in line strength have been included in the radiance scaling uncertainty mentioned above. Possible errors in linewidth were treated by assuming an uncertainty of 1.8 % in the broadening function and an uncertainty of 4 % in the temperature exponent. These uncertainties were estimated by combining information from *Bauer et al.* [1989] and *Goyette and De Lucia* [1990]. We also include a related uncertainty from imperfect knowledge of the Doppler shift of the emitted radiation, produced by line of sight velocity effects. Atmospheric wind along the line of sight will be the dominant source of error since both the spacecraft and earth velocity components are reasonably well known. An uncertainty of 70 m/s in line of sight velocity was assumed. The root-sum-square uncertainty in H_2O mixing ratio due to these three error sources is

generally less than 2%, although an uncertainty of 4% is produced at 0.46 hPa which is due to the uncertainty in line of sight velocity.

Dry air continuum. The dry air continuum is a semi-empirical contribution which is derived from radiance data from the 205 GHz radiometer (see *W. G. Read et al., paper in preparation*). Possible errors produced by imperfect knowledge of the dry air continuum are estimated by assuming that no dry air continuum is present in the forward model and by comparing the subsequent retrieved H_2O mixing ratios with a standard retrieval. This is a "worst case" scenario. The rms error in mixing ratio is estimated by dividing the worst case error by 3. This error source is only significant in the lower stratosphere where an uncertainty of $\sim$ 1.5% occurs at 46 hPa and an uncertainty somewhat less than 1% occurs at 22 hPa.

FOV shape and position. FOV shape and position errors of the 183 GHz radiometer have been transformed into errors in radiance [see *Jarnot et al.*, this issue]. A 1σ error of 0.5 K is assumed and a covariance matrix of radiance error due to this source was constructed assuming these errors to be fully correlated across the band. The resulting uncertainty in H_2O mixing ratio is generally less than 1%.

Filter shape. Each frequency channel across the H_2O band of the 183-GHz radiometer has an associated filter shape and position. Filter position errors are negligible, but errors in filter shape could give rise to worst case errors in calibrated radiance of $\sim$ 0.5% [see *Jarnot et al.*, this issue]. A covariance matrix of radiance error due to this source was constructed with no correlations between channels. The resulting uncertainty in H_2O mixing ratio is negligible compared to the other systematic uncertainties mentioned above.

Finally, we give an estimate of the total uncertainty in MLS H_2O derived from the estimated uncertainties, both random and systematic, mentioned above. We also include the smoothing error [*Marks and Rodgers*, 1993] which represents the contribution of the a priori errors to the retrieved uncertainty. As mentioned earlier for the averaging kernel calculation which enters into the smoothing error term, results may be somewhat different if a finer resolution grid for the true profiles is assumed. Mainly, the smoothing error could be somewhat larger in the region of good measurement sensitivity. Figure 13 shows the estimated precision (from method 3 above), the root-sum-square (rss) systematic uncertainty and the smoothing error along with the root-sum-square of these three uncertainties. In section 7 we give a summary table of the estimated precision (from method 3 above) and accuracy (rss error in Figure 13) for the useful vertical range of MLS version 3 H_2O data.

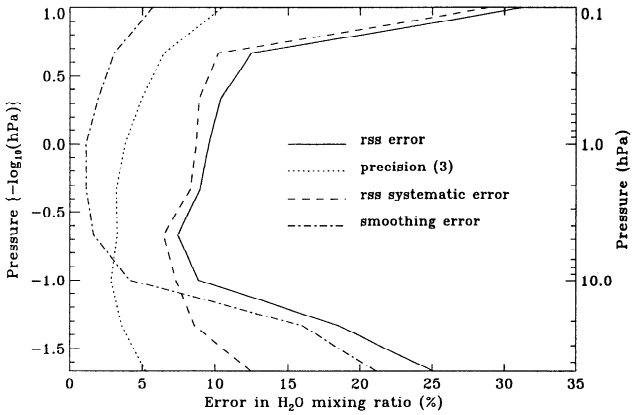

Figure 13. Estimated uncertainties associated with the retrieval of MLS H_2O: rss error, root-sum-square of precision, systematic error and smoothing error; precision (3), estimate of precision using method 3 (see text); rss systematic error, root-sum-square of estimated systematic errors; smoothing error, contribution of the a priori errors.

5. Comparison of MLS and Correlative Measurements

We now compare MLS H_2O data with measurements from four other observing systems. Two of these, a frost-point hygrometer and an infrared spectrometer are balloon mounted. The other two are a ground-based microwave spectrometer and a satellite-borne instrument which measures infrared absorption during solar occultations.

5.1. Frost Point Hygrometer Data

This instrument has an altitude range from the ground to $\sim$ 28 km with a vertical resolution of 250 m. The accuracy of these measurements is 10%; their precision is 10% in the stratosphere. The measurement sites which have have been used in this MLS-correlative comparison are: Boulder (40.0°N, 105.0°W), Hilo, Hawaii (19.7°N, 204.9°E), and Lauder, New Zealand (45.0°S, 109.4°E). Data were also taken during the Central Equatorial Pacific Experiment (CEPEX) at approximately (2.0°N, 157.5°W).

We have used the 12 balloon profiles distributed over these sites, for which there was coincident MLS water vapor data. Figure 14 shows a typical profile, taken in this case at Hilo. Some of the closest MLS profiles are shown for comparison. The two data sets overlap over a restricted height range; the balloon data and the MLS data can be usefully compared at the 22 and 46-hPa levels. We therefore calculated the differences between each balloon profile and the nearest MLS profile at these levels. At 46-hPa the mean difference (MLS–balloon), taken over these 12 comparisons, is 0.2 ppmv, while the root-mean-square difference is 0.5 ppmv. At 22 hPa the mean difference is 0.1 ppmv and the rms difference is 0.4 ppmv, the average being taken over the six balloon flights which reached a sufficient altitude for a comparison to be made at this level. We conclude that the systematic bias between the two data sets is smaller than 0.2 ppmv and that the random differences are within the quoted uncertainties. We note that none of the profiles used are at a latitude poleward of 45°.

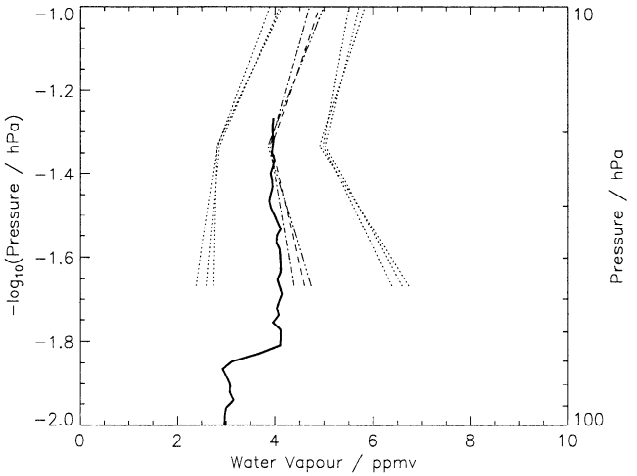

Figure 14. A typical water vapor profile measured by a balloon-mounted frost-point hygrometer (solid curve). The balloon was launched from a site in Hawaii at latitude 19.4°N, longitude 155°W, on March 24, 1991. Several MLS profiles for nearby locations are shown by dashed and dotted-dashed lines, their error bars are shown by dotted lines. The balloon profile is within the MLS errors at 46 and 22 hPa.

5.2. Ground-Based Microwave Data

This instrument is a ground-based water vapor millimeter wave spectrometer. All measurements used in this comparison have a vertical range between 30 and 80 km. The total absolute error of these measurements is $\sim$ 10 % over the height range 40–70 km [*Nedoluha et al.*, 1995]. This technique has a vertical resolution of $\sim$ 15 km. This is considerably coarser than the resolution of MLS so for a better comparison it would be desirable to smooth the MLS data using the averaging kernels of the ground-based instrument. We have not done this, so it should be borne in mind that MLS may detect features in the atmosphere which the ground-based instrument cannot resolve. The measurement site is Table Mountain Observatory (TMO), located at 34.4°N, 243.0°E, the data are a daily average and are provided with a pressure grid, the conversion from height to pressure having been performed using temperature and pressure fields from the National Meteorological Center (NMC) and the Middle Atmosphere Program (MAP) model [*Hedin*, 1991].

MLS version 3 data are compared with version 2 of the ground-based data in Figure 15, where we plot both the mean difference (MLS − ground based) and the rms difference. Data used in the comparison are from the period of January 23, 1992 to October 13, 1992; this period provided a total of 186 days on which both MLS and ground-based measurements were available. The rms difference is not much greater than the mean difference, suggesting that much of the difference between the two data sets is systematic. The ground based data is less accurate at lower altitudes; some of the difference at 2.2 hPa and perhaps at 1.0 hPa may be attributed to this. The MLS version 3 values at 0.46 and 0.22 hPa are probably too large by about 1 ppmv. The MLS version 3 value at 0.1 hPa is often as great as 10 ppmv. This is thought to be an artifact of the retrieval which we hope to remove in subsequent versions of the processing software. It is for this reason that we recommend that data from 0.1 hPa and above should not be used for scientific purposes.

5.3. Far Infrared Spectrometer (FIRS-2) data

This instrument is an infra-red emission Fourier transform spectrometer carried by a balloon [*Johnson et al.*, 1995]. Its vertical range is approximately 100–3 hPa, with a sampling interval of approximately 4 km, conveniently filling in the gap between the frost-point hygrometer and the ground-based microwave data sets. It made three flights during the period when the 183-GHz radiometer of MLS was operational, at times and places chosen to coincide with UARS limb-viewing measurements. Figure 16 shows a FIRS-2 profile and an MLS profile. As with the frost-point hygrometer data, the profiles agree well in the lower stratosphere. Furthermore, the MLS profile becomes greater than the FIRS-2 profile as height increases, suggesting that the difference between the ground-based microwave data and the MLS data is largely because MLS data are too high, rather than because the ground-based values are too low. These features are repeated in the other two FIRS-2 flights.

The MLS version 3 software cannot retrieve water vapour at 100-hPa. The values it produces are almost entirely climatological, but it is worth remarking that they are always too high when compared with correlative data. It will be possible, by using a nonlinear retrieval, to measure water vapor at this level; the com-

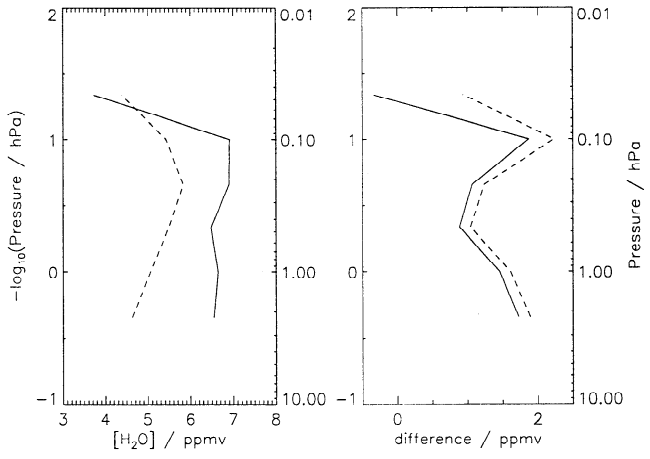

Figure 15. Comparison of MLS version 3 water vapour with the version 2 data from the ground-based microwave instrument. Data are from the period of January 23, 1992 to October 13, 1992; a total of 186 days for which both MLS and ground-based measurements were available. (left) Mean profiles; the solid curve is MLS data, the dashed curve ground-based. The (right) Mean difference, MLS − ground based (solid) and the rms difference (dashed).

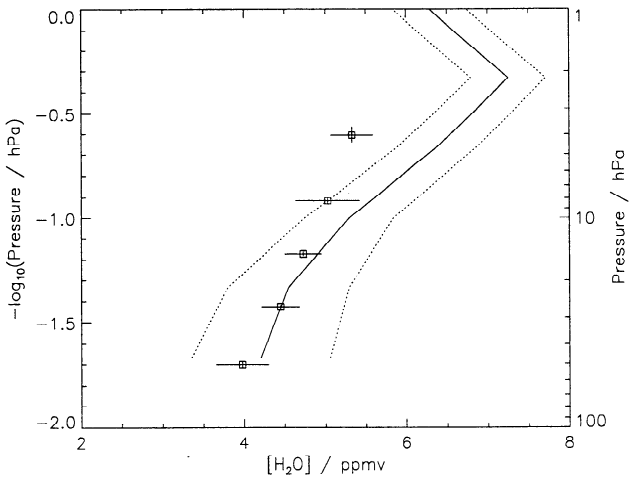

Figure 16. Water vapor profiles measured by MLS (solid curve) compared with FIRS-2 (squares) on September 29, 1992. The MLS profile is at latitude 37.5°N, longitude 103.2°W, the FIRS II profile is at latitude 36.9°N, longitude 100.4°W.

parison with correlative data suggests that a revised climatology is desirable before this is attempted. It is planned that future versions of the software will use a climatology which incorporates the SAGE II data set [*Rind et al.,* 1993].

5.4. Halogen Occultation Experiment (HALOE) data

In this section we present a comparison of MLS version 3 H_2O data with version 17 H_2O data from the HALOE instrument which is also onboard UARS. The Halogen Occultation Experiment (HALOE) is a limb-sounding instrument which measures atmospheric absorption of solar infrared radiation during sunrise and sunset events. The characteristics of the UARS orbit and the solar occultation combine to produce a coverage pattern giving 15 sunrise profiles at one particular latitude and 15 sunset profiles at a different latitude on each day. These profiles are spaced $\sim 24°$ apart in longitude with the latitude coverage changing throughout the year [*Russell at al.,* 1993]. HALOE is capable in clear air of measuring profiles from ~ 0.01 hPa to cloud top, i.e., the tropopause or lower. The overall accuracy of the HALOE version 17 H_2O profiles is estimated to be 20–25 % in the lower stratosphere, 10–15 % in the upper stratosphere and 15–20 % in the lower mesosphere. The vertical resolution of the HALOE profiles is ~ 2 km.

The differing coverage patterns of the HALOE and MLS instruments limit the latitudinal range and temporal extent of the comparison. During periods when the coverage patterns overlap, MLS data are used to build a representation of the way in which HALOE samples the atmosphere. These periods are normally around 20 days in duration. For each day within one of these periods, the average latitude of the HALOE profiles was calculated. Then, for the ascending and descending orbit modes of MLS, the profiles enveloping this average HALOE latitude were found. The corresponding MLS profile, for each orbit, at the average HALOE latitude was then obtained by linear interpolation. The zonal mean difference between the MLS profiles and the HALOE profiles (MLS–HALOE) was then calculated for each day of the comparison.

Figure 17 shows a contour plot of this zonal mean difference for the period January 21, 1993 to February 8, 1993. The latitudinal coverage for this comparison period is from 30°N at the beginning of the period to 50°S at the end of the period. The zonal mean difference is expressed in units of parts per million by volume. The comparison in Figure 17 uses MLS data from ascending orbit tracks only; however, similar features are produced when using data from descending orbit tracks. The results of this particular comparison are typical of those from other periods which have been studied.

In general, the zonal mean differences do not show any strong variation with latitude. In the lower stratosphere MLS and HALOE H_2O values differ by less than 0.5 ppmv (10 %) with MLS values tending to be larger than HALOE values. At 46 hPa the MLS values can be slightly less than those of HALOE. These differences are comparable with the H_2O error estimate produced by the MLS retrieval algorithms for this region of the atmosphere. In the upper stratosphere and lower mesosphere, MLS H_2O values are consistently higher than the HALOE values by 1.0–1.5 ppmv (10–20 %). These differences tend to be greater than the MLS error estimate and are also consistent with comparisons with other correlative measurements presented earlier in this section. At 0.1 hPa the MLS H_2O values can be as much as 3 ppmv (30 %) larger than the HALOE values. At this pressure level the MLS version 3 H_2O values are considered to be unphysically large (see section 6).

6. Topics for Future Work

While the version 3 water vapor is a useful quantity, there are some problems associated with it and improvements which can be made. Recent research [*Liebe et al.,* 1992] has shown that the oxygen lines used to retrieve temperature and pressure have a slightly smaller linewidth than was assumed in the version 3 software. Tests show that using the corrected linewidths gives somewhat lower values for water vapor in the stratosphere. The decrease is less than 0.2 ppmv in the lower stratosphere and is typically 0.3–0.5 ppmv in the upper stratosphere and tends therefore to bring the MLS water vapor into better agreement with the correlative measurements. Also, using the new oxygen linewidths gives rise to smaller discrepancies between measured and calculated radiances.

A serious problem is the loss of information which occurs at 46 and 22 hPa in the winter at polar latitudes. The information is lost because the version 3 software does not use radiances which come from ray paths which are judged to be optically thick. These radiances are related nonlinearly to the water vapor content so a nonlinear retrieval process would be required to make full

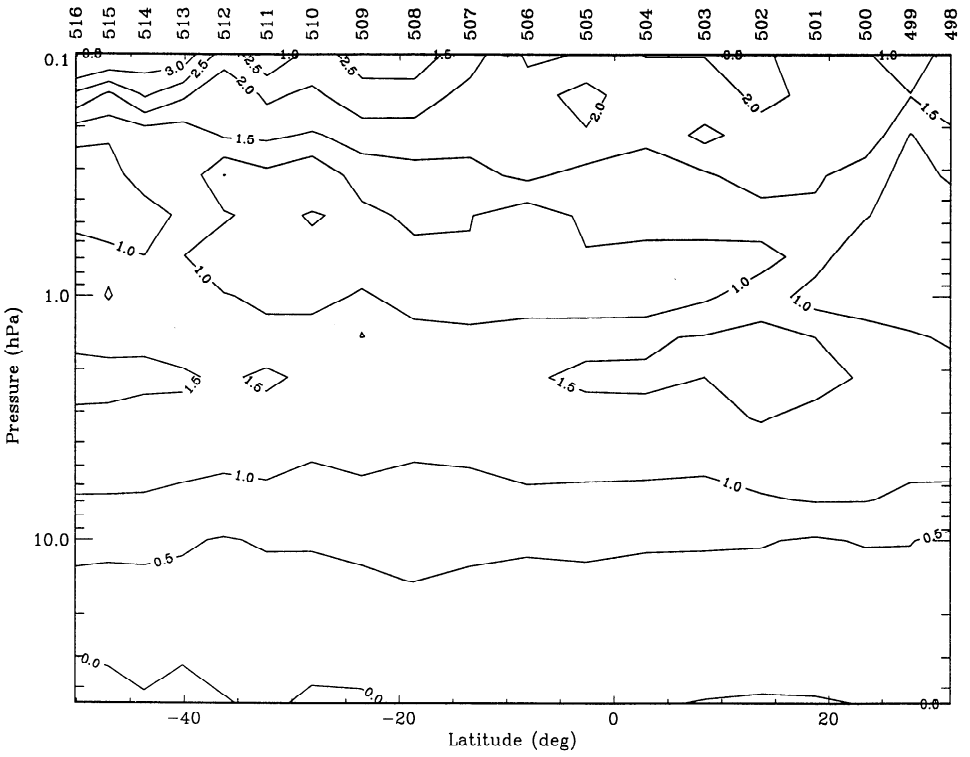

Figure 17. Zonal mean difference (MLS − Halogen Occultation Experiment(HALOE)) between MLS version 3 H_2O and HALOE version 17 H_2O for the period January 21, 1993 to February 8, 1993. The numbers along the top of the plot are the UARS day numbers for which each zonal mean difference profile was calculated. This comparison period begins on UARS day 498 (January 21, 1993) where the latitude of coincident MLS and HALOE measurements is ~ 30°N and the period ends on UARS day 516 (February 8, 1993) where the coincident latitude is 50°S. The MLS data used is from ascending orbit tracks only. The zonal mean differences are expressed in units of ppmv.

use of them. Tests have suggested that the criterion used in version 3 is rather stricter than necessary and that using a few more radiances than are used at present would make the retrieval better rather than worse. This cannot be implemented immediately because it causes other problems, particularly with the baseline.

The same tests suggest that a similar problem is at least partly responsible for the notch at 0.1 hPa. The center channel, channel 8, becomes optically thick and is not used at this level, while channels 7 and 9 only have sufficient signal to retrieve water vapor below this level.

With these changes, a future linear retrieval should be an improvement on the current version. However, to extract full information from the measurements will require a non-linear retrieval. Initial tests show that it is possible to retrieve water vapour at 100 hPa by this technique. It is also possible [*Read et al.*, 1995] to retrieve upper tropospheric water vapour from MLS band 3 (at 206 GHz), normally used for stratospheric chlorine monoxide. We plan to include this information along with that from the 183-GHz radiometer into a single retrieval process, producing a measurement of water vapor from the upper troposphere to the mesosphere.

In addition to these major changes, there are some minor artefacts in the data which we plan to eliminate. There are occasional profiles for which the retrieval has clearly failed but which are not flagged as being bad. One known cause occurs during the generation of calibrated radiances (level 1 data) and will be eliminated in future versions of the software. Another artefact occurs in the data at 22 hPa which show a small systematic dependence on the UARS yaw cycle. This effect is not fully understood at present but is clearly an artefact which needs to be removed. An important improvement will be the use of a revised climatology; the current version is supplying unsuitable a priori values at 100 hPa. Finally, tracer transport studies [*Manney et al.*, 1995] suggest that MLS water vapour in the upper stratosphere does not behave like a passive tracer. We aim to establish whether this is an artefact of the retrieval or the tracer transport code or whether it is a real physical effect.

7. Estimated Accuracy and Precision of MLS Version 3 Data

MLS version 3 H_2O retrievals give reasonable values in the stratosphere but consistently overestimate other correlative measurements. The current range of useful sensitivity (as measured by the data quality; see section 4) is between 46 hPa and 0.01 hPa, although lower-

Table 1. Microwave Limb Sounder Version 3 H_2O Data Summary

UARS Standard Levels	Pressure, hPa	Single Profile Precision *		Accuracy †	
		ppmv	percent	ppmv	percent
22	0.22	0.45	7	0.9	13
20	0.46	0.33	5	0.7	11
18	1	0.25	4	0.7	10
16	2.2	0.20	3	0.6	9
14	4.6	0.17	3	0.5	8
12	10	0.13	3	0.5	9
10	22	0.14	4	0.8	19
8	46	0.20	5	1.2	25

*The estimated precisions are based on the observed variability of retrievals in the tropics (see section 4.3).

†The estimated accuracies are based on the error analysis presented in section 4.

mesospheric retrievals appear suspect at present due to a 'notch' around ~ 0.1 hPa (see section 6). Retrievals at 46 hPa in the polar winter can have poor data quality (see section 2). Therefore, the recommended pressure range for scientific studies using MLS H_2O is from 22 hPa to 0.2 hPa for all latitudes and from 46 hPa to 0.2 hPa at the tropics and midlatitudes.

Comparison with other H_2O measurements suggests that MLS H_2O values are too high by ~ 5 % at 46 and at 22 hPa and by 15–20 % in the range 1 to 0.22 hPa.

The characteristics of MLS H_2O 183 GHz measurements retrieved using version 3 of the software are summarized in Table 1. The precision estimates in Table 1 may be slightly pessimistic as they are based on the observed variability of retrieved profiles in the tropics and may contain effects of atmospheric variability. The estimates of accuracy in Table 1 contain the effects of systematic uncertainties, the contribution of the a priori error to the retrieved uncertainty and the above mentioned precision estimates. In the pressure range 1 to 0.22 hPa the estimated accuracy in Table 1 does not fully account for the differences found in the comparisons with correlative data. This suggests that some systematic effects may not be accounted for in the error analysis of section 4.

Acknowledgments. We thank many colleagues, at Edinburgh University, Heriot-Watt University and the Rutherford Appleton Laboratory in the United Kingdom and at the Jet Propulsion Laboratory in the United States, who have contributed to the MLS project. We are indebted to various persons from the UARS project and elsewhere for the compilation of data and model values which make up the "UARS Climatology File," which is used as a priori information in the MLS retrieval process; in particular, we acknowledge the efforts of R. Seals and P. Connell. We also thank M. Allen for the default model profiles used as part of this procedure. Early simulations of MLS retrievals also benefited from the availability of three-dimensional model results, made possible by W. L. Grose and G. Lingenfelser, at the NASA Langley Research Center. We thank the groups at NOAA Climate Monitoring and Diagnostics Laboratory, the Naval Research Laboratory, Harvard-Smithsonian Center for Astrophysics, and NASA Langley Research Center for kindly providing correlative data sets. We also acknowledge the useful comments of B. Connor. The work in the United Kingdom was funded by SERC and NERC, and in the United States by NASA.

References

Backus, G. E., and J. F. Gilbert, Uniqueness in the inversion of inaccurate gross Earth data, *Philos. Trans. R. Soc. London A, 266*, 123–192, 1970.

Barath, F. T. et al., The Upper Atmosphere Research Satellite microwave limb sounder instrument, *J. Geophys. Res., 98*, 10,751–10,762, 1993.

J. J. Barnett, and M. Corney, Handbook for Middle Atmosphere Program (MAP), SCOSTEP Sec., Univ. of Ill., Urbana, 1989.

Bauer, A., M. Godon, M. Kheddar, and J. M. Hartmann, Temperature and perturber dependences of water vapor line-broadening: Experiments at 183 GHz; calculations below 1000 GHz, *J. Quant. Spectrosc. Radiat. Transfer 41(1)*, 49–54, 1989.

Bevilacqua, R. M., W. J. Wilson, W. B. Ricketts, P. R. Schwartz, and R. J. Howard, Possible seasonal variability of mesospheric water vapor, *Geophys. Res. Lett., 12*, 397–400, 1985.

Bevilacqua, R. M., W. J. Wilson, and P. R. Schwartz, Measurements of mesospheric water vapor in 1984 and 1985: Results and implications for middle atmospheric transport, *J. Geophys. Res., 92*, 6679–6690, 1987.

Bevington, P. R., *Data Reduction and Error Analysis for the Physical Sciences*, McGraw-Hill, New York, 1969.

Fishbein, E. F. et al., Validation of UARS microwave limb sounder temperature and pressure measurements, *J. Geophys. Res.*, this issue.

Froidevaux, L. et al., Validation of UARS microwave limb sounder ozone measurements, *J. Geophys. Res.*, this issue.

Goyette, T. M., and F. C. De Lucia, The pressure broadening of the $3_{1,3}$–$2_{2,0}$ transition of water between 80 K and 600 K, *J. Mol. Spectrosc. 143(2)*, 346–358, 1990.

Hedin, A. E., Extension of the MSIS thermosphere model into the middle and lower atmosphere, *J. Geophys. Res., 96*, 1159–1172, 1991.

Jarnot, R. F. et al., Calibration of the microwave limb sounder on UARS, *J. Geophys. Res.*, this issue.

Johnson, D. J., K. W. Jucks, W. A. Traub, and K. V. Chance, The Smithsonian stratospheric far-infrared spectrometer and data reduction system, *J. Geophys. Res., 100*, 3091–3106, 1995.

Liebe, H. J., P. W. Rosenkranz, and G. A. Hufford, Atmospheric 60 GHz oxygen spectrum: New laboratory mea-

surements and line parameters, *J. Quant. Spectrosc. Radiat. Transfer, 48*, 629–643, 1992.

Manney, G. L., R. W. Zurek, W. A. Lahoz, R. S. Harwood, J. C. Gille, J. B. Kumer, J. L. Mergenthaler, A. E. Roche, A. O'Neill, R. Swinbank, and J. W. Waters, Lagrangian transport calculations using UARS data. Part I: Passive tracers, *J. Atmos. Sci., 52,* 3049–3068, 1995.

Marks, C. J., and C. D. Rodgers, A retrieval method for atmospheric composition from limb emission measurements, *J. Geophys. Res., 98*, 14,939–14,953, 1993.

Nedoluha, G. E., R. M. Bevilacqua, R. M. Gomez, D. L. Thacker, W. B. Waltman, and T. A. Pauls, Ground-based measurements of water vapor in the middle atmosphere, *J. Geophys. Res., 100*, 2927–2939, 1995.

Pickett, H. M., R. L. Poynter, and E. A. Cohen, Submillimeter, millimeter and microwave spectral line catalog, *JPL Tech. Rep. 8023,* revision 3, Jet Propul. Lab., 1992.

Read, W. G., J. W. Waters, D. A. Flower, L. Froidevaux, R. F. Jarnot, D. L. Hartmann, R. S. Harwood, and R. B. Rood, Upper-Tropospheric Water Vapor from UARS MLS, *Bull. Am. Meteorol. Soc., 76,* 2381–2389, 1995.

Reber, C. A., The Upper Atmosphere Research Satellite *Eos Trans. AGU 71(51)*, 1867–1868, 1873–1874, 1878, 1990.

Remsberg, E. E., J. M. Russell III, and C.-Y. Wu, An interim reference model for the variability of the middle atmosphere water vapor distribution, *Adv. Space Res., 10*, 51–64, 1990.

Rind, D., E.-W. Chiou, W. Chu, S. Oltmans, J. Lerner, J. Larsen, M. P. McCormick, and L. McMaster, Overview of the Stratospheric Aerosol and Gas Experiment II water vapour observations: Method, validations and data characteristics, *J. Geophys. Res., 98*, 4835–4856, 1993.

Rodgers, C. D., Retrieval of atmospheric temperature and composition from remote measurements of thermal radiation, *Rev Geophys., 14*, 609–624, 1976.

Rodgers, C. D., Characterization and error analysis of profiles retrieved from remote sounding measurements, *J. Geophys. Res. 95*, 5587–5595, 1990.

Russell, J. M. III, J. C. Gille, E. E. Remsberg, L. L. Gordley, P. L. Bailey, H. Fischer, A. Girard, S. R. Drayson, W. F. J. Evans, and J. E. Harries, Validation of water vapor results measured by the limb infrared monitor of the stratosphere (LIMS) experiment on NIMBUS 7, *J. Geophys. Res., 89*, 5115–5124, 1984.

Russell, J. M. III, L. L. Gordley, J. H. Park, S. R. Drayson, W. D. Hesketh, R. J. Cicerone, A. F. Tuck, J. E. Frederick, J. E. Harries, and P. J. Crutzen, The Halogen Occultation Experiment, *J. Geophys. Res., 98*, 10,777–10,797, 1993.

Tsou, J-J., J. J. Olivero, and C. L. Croskey, Study of variability of mesospheric H_2O during spring 1984 by ground-based microwave radiometric observations, *J. Geophys. Res., 93*, 5255–5266, 1988.

Waters, J.W., Absorption and emission by atmospheric gases, in *Methods of Experimental Physics, 12B*, (edited by L. Meeks), pp. 142–176, Academic, San Diego, Calif., 1976.

Waters, J. W., Microwave limb sounding, in *Atmospheric Remote Sensing by Microwave Radiometry,* (edited by M.A. Janssen), chap. 8, John Wiley, New York, 1993.

Waters, J. W. et al., Validation of UARS MLS ClO measurements, *J. Geophys. Res.,* this issue.

L. Froidevaux, T. A. Lungu, W. G. Read, Z. Shippony, and J. W. Waters, Jet Propulsion Laboratory, California Institute of Technology, Pasadena, CA 91109 (email: lucien@camel.jpl.nasa.gov, lungu@camel.jpl.nasa-.gov, bill@camel.jpl.nasa.gov, zvi@camel.jpl.nasa.gov, joe@-camel.jpl.nasa.gov

R. S. Harwood, H. C. Pumphrey (corresponding author), and M. R. Suttie, Department of Meteorology, Edinburgh University, Scotland, EH9 3JZ (email: R.S.Harwood@-ed.ac.uk, H.C.Pumphrey@ed.ac.uk, Martin.Suttie@mail.-esrin.esa.it

W. A. Lahoz, CGAM, Department of Meteorology, Reading University, England, RG6 2AU. (email: wal@met.-reading.ac.uk)

C. L. Lau, G. E. Peckham, and R. A. Suttie, Department of Physics, Heriot-Watt University, Edinburgh, Scotland, EH14 4AS (email: lau@phy.hw.ac.uk, PHYGEP@-clust.hw.ac.uk, suttie@phy.hw.ac.uk

G. E. Nedoluha, Naval Research Laboratory, Code 7220, Washington, D. C. 20375 (email: nedoluha@rira.nrl.-navy.mil)

S. J. Oltmans, NOAA Climate Monitoring and Diagnostics Laboratory, Boulder, CO 80303 (email: soltmans@-cmdl.noaa.gov)

J. M. Russell III, NASA Langley Research Center, Hampton, VA 23665

W A. Traub, Harvard-Smithsonian Center for Astrophysics, Cambridge, MA 02138

(Received November 19, 1994; revised April 15, 1995; accepted May 27, 1995.)